Phase separation of rigid-rod suspensions in shear flow

Peter D. Olmsted[1,*] and C.-Y. David Lu[2,†]
[1]*Department of Physics, University of Leeds, Leeds LS2 9JT, United Kingdom*
[2]*Department of Physics and Center of Complex Systems, National Central University, Chung-li 320, Taiwan*
(Received 16 April 1999)

We analyze the behavior of a suspension of rigid-rod-like particles in shear flow using a modified version of the Doi model, and construct diagrams for phase coexistence under conditions of constant imposed stress and constant imposed strain rate, among paranematic, flow-aligning nematic, and log-rolling nematic states. We calculate the effective constitutive relations that would be measured through the regime of phase separation into shear bands. We calculate phase coexistence by examining the stability of interfacial steady states and find a wide range of possible ''phase'' behaviors. [S1063-651X(99)06810-5]

PACS number(s): 83.70.Jr, 64.70.Md, 83.20.Hn, 64.10.+h

I. INTRODUCTION

Shear flow has profound effects on complex fluids. It can perturb equilibrium phase transitions, such as the isotropic-to-nematic (*I*-*N*) liquid crystalline transition in wormlike micelles [1–3], thermotropic melts [4–7], or rigid-rod suspensions [8,9]; the nematic-smectic transition in thermotropic liquid crystals [10]; and the isotropic-to-lamellar transition [11] in surfactant systems. Shear can also induce structures, such as the well-known multilamellar vesicles (onions) in surfactant systems [12–14], that exist only as metastable equilibrium phases. Another well-known effect is the transition between orientations of diblock copolymer lamellae in either the steady shear flow [15,16], or the oscillatory shear flow [17–19], as a function of shear rate or frequency, and temperature.

A related phenomenon is dynamic instability in non-Newtonian fluids whose theoretical *homogeneous* stress–strain-rate constitutive relations exhibit multivalued behavior, as in theories of polymer melts [20,21] and wormlike micelles [22–24]. Such models may describe, for example, the spurt effect, whereby the flow rate of a fluid in a pipe changes discontinuously as a function of applied pressure drop [25]. A nonmonotonic constitutive curve as in Fig. 1 typically has a segment (shown as a broken line) where bulk flow is unstable. If a mean strain rate is imposed which forces the system to lie on an unstable part of the constitutive relation, a natural resolution for this instability is to break the system into two regions, often called *bands*, one on the high strain rate branch and one on the low strain-rate branch, to maintain the overall applied strain rate. The most important unresolved question about these banded flows is, what determines the stress at which the system phase separates into bands? Experiments on many systems (reviewed in Sec. II A), particularly the wormlike micelle surfactant systems, reveal that there is a well-defined and reproducible selected stress in a wide class of systems.

There have been many suggestions for determining the selected stress. Some workers have assumed the existence of a nonequilibrium potential and a variational principle [26,27]. This possibility is intriguing, although it remains unproven. Early studies postulated a jump at the top of the stable viscous branch (''top jumping'') [21,22,28], but experiments have shown that this is not the case [29]. Recent studies have solved the homogeneous flow equations in various geometries using sophisticated hydrodynamic flow-solvers and found a selected stress [30,31]. However, evidence is growing [32] that these calculations have history-dependent stress selection (which is in fact no selection) or introduce gradient terms due to the discretization of the system. A final method, which we follow here, has been to incorporate (physically present) nonlocal contributions to the stress [5,6,33,34,9,32,35–37], and examine the equations of motion under steady banded flow conditions.

Here we extend previous work [9] and calculate phase diagrams for rigid-rod suspensions in shear flow, solving for the interfacial profile between phases and using its properties to determine the coexistence stress. As Fig. 1 indicates, phase separation is possible at *either* a specified stress (horizontal tie lines) *or* a specified strain rate (vertical tie lines). Only recently has the latter possibility been speculated upon

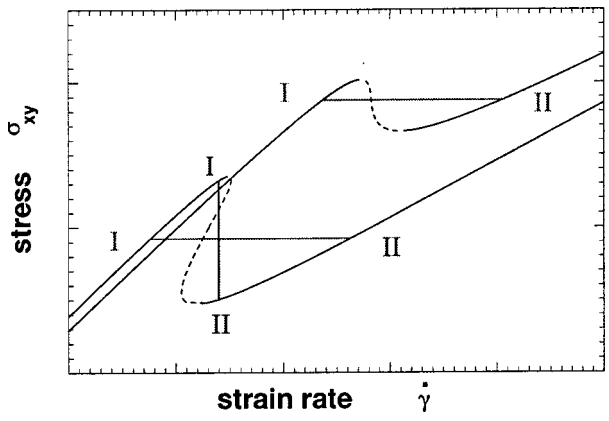

FIG. 1. Stress–strain-rate curves for the Doi model with different excluded volume parameters *u* (taken from Fig. 3 below). The dashed line segments are unstable (unphysical) steady states. The straight lines indicate possible coexistence between states *I* and *II* under conditions of common stress (horizontal lines) or strain rate (vertical line).

*Electronic address: p.d.olmsted@leeds.ac.uk
†Electronic address: dlu@joule.phy.ncu.edu.tw

[28,9,27], and found experimentally [38]. We explore this possibility explicitly for our model system, which possesses, in addition to the high and low strain-rate (paranematic and nematic, respectively) branches shown in Fig. 1, a second high strain-rate branch in which the rods stand up in the flow, parallel to the vorticity direction, instead of lying in the shear plane [39]. We study coexistence with this so-called ''log-rolling'' phase and find a rich nonequilibrium phase diagram.

The summary of this paper is as follows. In Sec. II we discuss the general issues of shear banding and phase separation in flow, and summarize the primary experimental evidence for this behavior. In Sec. III we present the modified Doi model [40,41] and in Sec. IV we briefly discuss our algorithm for calculating the phase diagram. The general aspects of the interface construction will be discussed elsewhere [35]. We present the results for common stress- and strain-rate phase separation in Secs. V and VI, respectively, and discuss some of the implications for metastability and experiments under controlled stress or controlled strain-rate conditions. We finish in Sec. VII with a discussion and summary. While some of these results have been briefly summarized elsewhere [42], the current paper is a complete and self-contained discussion of the problem.

The reader interested in the phenomenology of phase diagrams for sheared complex fluids rather than liquid crystals may safely skip Sec. III; the rest of the paper is general, and much of the discussion applies to any system undergoing phase separation in shear flow. There are, essentially, two steps to calculating phase behavior in flow. One must derive the dynamical equations of motion for fluid flow, composition, and the relevant structural order parameter(s), which is quite difficult. Then, one must understand how to solve them and interpret the results. While the modified Doi model does not exhaust all possible phase diagrams (in particular, a shear-thickening model would be a nice complement), it has many universal features. One extremely important concept is that density and field variables are ill-defined in nonequilibrium systems: *either* stress *or* strain rate may act as a control parameter analogous to an equilibrium field variable (e.g., pressure, chemical potential), corresponding to the different orientations of the interface between coexisting phases. Also, one can gain much intuition from the underlying stress–strain-rate–composition *surface*, a fact which we feel has been underappreciated until now.

II. SHEAR BANDING

A. Experimental evidence

Shear banding has been confirmed in many systems through direct optical and NMR visualization, and deduced from rheological measurements. The best-studied systems are surfactant solutions of various kinds, including wormlike micelles and onion-lamellar phases. Rehage and Hoffmann [24] measured a plateau in the stress–strain-rate relation for wormlike micelles in shear flow. This behavior has since been seen in a number of wormlike micellar systems in various flow geometries, by the Montpellier [1–3], Strasbourg [43], Edinburgh [29], and Massey groups [44–47]. Berret *et al.* [3] visualized shear bands in the plateau region of the stress–strain-rate curves using optical techniques, providing proof of banding; and Callaghan *et al.* [44–47] used NMR to measure the velocity profile in various geometries (including Couette, cone-and-plate, and pipe geometries).

The transition in these cases is to a strongly aligned, possibly nematic, phase of wormlike micelles which has a lower viscosity than the quiescent phase. It is not known how the length distribution changes in flow, although this is certainly an important aspect of these ''living'' systems [48]. Wormlike micellar system can possess an equilibrium nematic phase, and in some cases the shear-induced phase is obviously influenced by the proximity of an underlying nematic phase transition [1,2,49,3,50]. However, many wormlike micellar systems undergo banding at compositions much more dilute than that for I-N coexistence, and it is probable that in these cases flow instability is due to the nonlinear rheology of these systems, which is in many respects similar to that of the Doi-Edwards model of polymer melts [23]. Since there are at lease two possible effects (a nematic phase transition and flow instability of the micellar constitutive relation) apparently leading to flow instability, these systems are quite rich. It is tempting to analyze the extent to which these systems display behavior analogous to the kinetics of equilibrium phase separation, and groups have recently begun to study the kinetics of nonequilibrium phase separation [2,29,51].

Pine and co-workers have recently studied a wormlike surfactant system at extreme dilutions and found, surprisingly, that for low enough concentrations (but still above the overlap concentration) shear induces a viscoelastic phase that they interpret as a gel [52–54]. The origins and structure of this gel are currently unknown. In controlled stress experiments they observe shear banding and a ''plateau'' for stresses higher than a certain stress, in which the strain rate *decreases* as shear induces the gel. Above the stress at which the gel fills the sample cell, the strain rate increases again to complete a dramatic S curve. For controlled strain-rate experiments the system jumps, at a well defined strain rate, between the gel and solution phases.

Another well-studied system is the onion lamellar surfactant phase, originally studied by Roux, Diat, and Nallet [12–14]. These systems display a bewildering variety of transitions between lamellar, aligned-lamellar, onion, and onion crystal phases of various symmetries, as functions of applied shear flow, temperature, and composition. As an example, one particular system undergoes transitions, with increasing strain rate, from disordered lamellae to onion, to onion-lamellae coexistence (in which coexistence is inferred from a plateau in the stress–strain-rate curves), to well-ordered lamellae [13]. Recently, Bonn and co-workers [38] found shear-induced transitions between different gel states of lamellar onion solutions with shear bands (visualized by inserting tracer particles) oriented with interface normals in the vorticity direction, indicating phase separation at common strain rate instead of common stress, as we clarify below. In this case the averaged stress–strain-rate constitutive relation followed a sideways S curve under controlled strain-rate conditions.

Mather *et al.* [7] have recently studied a thermotropic polymer liquid crystal using visual and rheological measurements, and inferred a shear-induced nematic phase transition

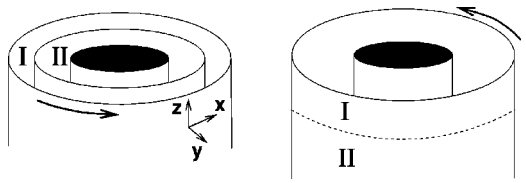

FIG. 2. Geometries for phase separation at common stress (left) or strain-rate (right) in a Couette rheometer. For phase separation at a common stress (left) phases *I* and *II* have different strain rates, while at a common strain rate (right) they have different stresses. $\hat{\mathbf{z}}$ is the vorticity axis, $\hat{\mathbf{x}}$ is the flow direction, and $\hat{\mathbf{y}}$ is the flow gradient axis.

and phase separation, the latter which they attribute to polydispersity.

In summary, shear-banding has been seen in several systems, and in all cases is associated with some flow-induced change in the fluid microstructure. Most systems are still poorly understood [52,14,38] and, given the range of complexity, it is certain that many qualitatively new phenomena remain to be discovered.

B. Theoretical issues

The crux of the problem from a theoretical point of view may be appreciated from Fig. 1. These stress–strain-rate curves are somewhat reminiscent of pressure-density (p-ρ) isotherms for a liquid-gas system. Curve segments with negative slope, $\partial\sigma_{xy}/\partial\dot{\gamma}<0$, are unstable and cannot describe a physical state of a bulk homogeneous system. Analogously, isotherms with negative slopes $\partial p/\partial\rho<0$ have negative bulk moduli and are unstable. The liquid-gas system resolves this instability by phase-separating into regions of different densities (according to the lever rule to maintain the average density). Similarly, the banded flows seen in the experiments described above appear to be a nonequilibrium phase separation into regions of high and low strain-rate, maintaining the applied mean strain rate.

In previous work [5,6,9] we constructed a ''phase diagram'' by pursuing an analogy between homogeneous stable steady states and equilibrium phases. As in equilibrium, nonequilibrium ''phases'' may be separated, in field variable space, by hypersurfaces representing continuous (e.g., critical points/lines) or discontinuous (''first-order'') transitions. Coexistence implies an inhomogeneous state spanning separate branches of the homogeneous flow curves. Note, however, that there is an ambiguity in connecting separate branches of the homogeneous flow curves in Fig. 1. The top curve permits coexistence of states with the same stress and different strain rates, while the lower curve also allows coexistence of states with the same strain rate and different stresses [28,9].

Figure 2 shows that phase separation at a common stress occurs such that the interface between bands is parallel to the vorticity-velocity plane (annular bands, in Couette flow), while phase separation at a common strain rate occurs with the interface between bands parallel to the velocity–velocity-gradient plane (stacked disks, in Couette flow).

This highlights a striking contrast between equilibrium and nonequilibrium systems. In equilibrium the field variables (pressure, temperature, chemical potential) are uniquely defined and determine phase coexistence. In sheared fluids, one needs an extra field variable to determine the extended phase diagram. However, *for a system with more than one choice of coexisting geometry, the appropriate field variable may not necessarily be identified a priori*. The complete answer of how to determine (theoretically) the dynamic field variable is not known. Of course, the nature of the constitutive relation may help, for example the top curve of the Fig. 1 does not allow the strain rate as the field variable. We will come back to discuss some possible answers to this interesting problem in Sec. VII B (see also [28] for other suggestions).

Another important difference from equilibrium systems is evident when, say, assuming the systems choose to form shear bands at common stress, we try to determine at which stress a system forms shear bands. The constitutive relations shown in Fig. 1 are calculated for homogeneous states, and there is no apparent prescription for determining the selected banding stress, despite the experimental evidence for a selected stress. A similar apparent degeneracy occurs in first-order phase transitions in equilibrium statistical mechanics, but is easily resolved by demanding that the system minimize its total free energy, or, equivalently, by appealing to the convexity of the free energy of the equilibrium thermodynamic systems [55]. This leads to equality of field variables between two phases and the common tangent condition (e.g., the Maxwell equal areas construction for liquid-gas coexistence [56], or the equal osmotic pressure condition, aided by equal chemical potential, in rod suspensions [57]).

In the shear band problem, an unambiguous resolution of this degeneracy is to consider the full *inhomogeneous* (i.e., nonlocal in space) equations of motion, and determine phase coexistence by that choice of field variables (appropriately chosen by hand) for which there exists a *stationary* interfacial solution to the steady-state differential equations of motion [5,34,9]. For zero stress this technique reduces, as it should, to minimization of the free energy. The importance of inhomogeneous terms in fluid equations of motion has been noted by several groups, who pointed out that the standard fluid equations can have ill-defined mathematical solutions [58] if such terms are not included. Of course, if the phase diagram depends sensitively on the form or magnitude of the inhomogeneous terms, one needs a detailed understanding of the underlying physics. The use of a stable interface to select among possible coexisting states was first postulated for nonlinear dynamical systems, as far as we know, by Kramer [59], and later by Pomeau [60], and was first applied (independently) to complex fluids in Ref. [6]. The inclusion of gradient terms in constitutive relations is rapidly gaining acceptance, as recent unpublished work by Goveas (phase separation of model blends of long and short polymers) [36] and Dhont (introduction of model gradient terms to resolve stress selection) [37] indicates.

In this work we study a model for rigid-rod suspensions in shear flow. While there are certainly ongoing experiments on these systems [7], the primary motivation for this extended work is to explore the manner in which phase separation and coexistence occurs in complex fluids in flow. The approximations used in obtaining our equations are severe (including a decoupling approximation whose defects are well-known [61]), and we expect qualitative agreement at best.

However, this is the first complete study of which we are aware of nonequilibrium phase separation of a complex fluid in flow for a concrete model, and we hope it illuminates the phenomenology of flow-induced phase transitions.

III. METHODOLOGY

We seek the equations of motion for a solution of rodlike particles. The most useful dynamic variables describing the long-wavelength hydrodynamic degrees of freedom are the volume fraction $\phi(\mathbf{r})$, the fluid velocity $\mathbf{v}(\mathbf{r})$, and the nematic order parameter tensor

$$Q_{\alpha\beta}(\mathbf{r}) = \langle \nu_\alpha \nu_\beta - \tfrac{1}{3}\delta_{\alpha\beta} \rangle, \tag{3.1}$$

where $\boldsymbol{\nu}$ is the rod orientations and $\langle\ \rangle$ denotes an average around the point $\mathbf{r}$. Previous studies of liquid crystals under shear flow have been either for thermotropics [5,6], where the issues we present below associated with composition coupling are not present, or homogeneous suspensions [8,39], where phase coexisting was not considered.

Our work below is based on the model extending that of Doi [40,41]. See *et al.* [8] studied the Doi model in shear flow, but did not attempt to consider phase coexistence. Bhave, *et al.* [39] analyzed this model in more detail, but did not consider realistic phase-separation behavior. We augment this model with reasonable estimates for translational entropy loss upon phase separation and for the free-energy cost due to spatial inhomogeneities. Zubarev studied shear-induced phase separation in a variation of the Doi model in flow based on the equality of nonequilibrium free energies, calculated from the flow-perturbed orientational distribution function [26]. Zubarev only considered phase separation at a common strain rate, and did not treat the rheological response (stress) of the system or log-rolling states.

A. Equations of motion

The free energy (e.g., as in Ref. [57]) is given by

$$\begin{aligned}\mathcal{F}(\phi,\boldsymbol{Q}) = k_B T \int d^3 r \Big\{ & \frac{\phi}{v_r}\ln\phi + \frac{(1-\phi)}{v_s}\ln(1-\phi) \\ & + \frac{\phi}{v_r}\big[\tfrac{1}{2}(1-\tfrac{1}{3}u)\,\mathrm{Tr}\,\boldsymbol{Q}^2 - \tfrac{1}{3}u\,\mathrm{Tr}\,\boldsymbol{Q}^3 + \tfrac{1}{4}u(\mathrm{Tr}\,\boldsymbol{Q}^2)^2 \\ & + \tfrac{1}{2}K(\nabla_\alpha Q_{\beta\lambda})^2\big] + \tfrac{1}{2}\frac{g}{v_s}(\nabla\phi)^2 \Big\}. \end{aligned} \tag{3.2}$$

Here, ''Tr'' denotes the trace, v_r and v_s are rod and solvent monomer volumes, and

$$u \equiv \nu_2 c d L_0^2 \tag{3.3}$$

is Doi's excluded volume parameter [40,41], where c is the concentration (number/volume) of rods of length L_0 and diameter d, and ν_2 is a geometrical prefactor (Ref. [40] estimated $\nu_2 = 5\pi/16 \simeq 0.98$). The volume fraction ϕ is

$$\phi = c v_r, \tag{3.4}$$

in terms of which

$$u = \phi L \frac{\nu_2}{\alpha}, \tag{3.5}$$

where $L = L_0/d$ is the rod aspect ratio and α is an $O(1)$ prefactor defined by

$$v_r = \alpha d^2 L_0. \tag{3.6}$$

For spherocylinders, $\alpha = \pi[1 - 1/(3L)]/8$, which reduces, in the limit $L \to \infty$, to $\alpha = \pi/8 \simeq 0.39$. We use u and ϕ interchangeably below as a composition variable.

In much of what follows, we make two further assumptions to reduce the number of parameters in our model. We fix v_s by assuming

$$v_r = L v_s, \tag{3.7}$$

which corresponds to a particular volume of the solvent molecules relative to that of the rodlike molecules. Further, we assume that the geometric factor ν_2/α has the value unity, so that

$$u = \phi L, \tag{3.8}$$

which corresponds to a particular shape of the rigid-rod molecules. These two assumptions specify the detailed shape and volume ratio of the system we study below. For slightly different systems with $v_r \neq L v_s$ or $\nu_2/\alpha \neq 1$, our work should still provide an accurate qualitative picture.

The first two terms of Eq. (3.2) comprise the entropy of mixing, and the first three terms in square brackets are from Doi's expansion of the free energy (derived per solute molecule) in powers of the nematic order parameter $\boldsymbol{Q}$. These terms were derived from the Smoluchowski equation for the distribution function of rod orientations [40,41]. We keep the expansion to fourth order to describe a first-order transition and give the correct qualitative trends.

Assuming Eqs. (3.7) and (3.8), we calculate the following biphasic coexistence regions:

$$\{u_I = 2.6925, u_N = 2.7080\} \quad (L = 5.0), \tag{3.9}$$

$$\{u_I = 2.6930, u_N = 2.7074\} \quad (L = 4.7), \tag{3.10}$$

where u_I and u_N are the excluded volume parameters (compositions) for the coexisting isotropic and nematic phases, respectively. Note the very weak dependence of the biphasic regime (in the scaled variable $u = L\phi$) on L.

The last two terms in Eq. (3.2) penalize spatial inhomogeneities. By adding the single term proportional to K we have assumed a particular relation for the Frank constants, $(K_1 = K_2 = K, K_3 = 0)$ [62,63]. Although Odijk has calculated these constants for model liquid crystals (in the nematic regime) [64], we will see below that this choice is probably unimportant for this model. More generally, we expect the Frank constants to vary as functions of $\boldsymbol{Q}(r)$ in physical systems, a situation which we have not addressed here. The final term penalizes composition gradients [65]. We are not aware of any calculations of g for solutions of rodlike particles. In Eq. (3.2), we assume an athermal solution with no explicit interaction energy.

The nematic order parameter obeys the following equation of motion [40,41]:

$$(\partial_t+\mathbf{v}\cdot\boldsymbol{\nabla})\boldsymbol{Q}=\boldsymbol{F}(\boldsymbol{\kappa},\boldsymbol{Q})+\boldsymbol{G}(\phi,\boldsymbol{Q}), \tag{3.11}$$

where $\kappa_{\alpha\beta}=\nabla_\beta v_\alpha$. In Eq. (3.11) the (reactive) ordering term $\boldsymbol{F}$ is given by

$$\boldsymbol{F}(\boldsymbol{\kappa},\boldsymbol{Q})=\tfrac{2}{3}\boldsymbol{\kappa}^s+\boldsymbol{\kappa}\cdot\boldsymbol{Q}+\boldsymbol{Q}\cdot\boldsymbol{\kappa}^T-2(\boldsymbol{Q}+\tfrac{1}{3}\boldsymbol{I})\mathrm{Tr}(\boldsymbol{Q}\cdot\boldsymbol{\kappa}), \tag{3.12}$$

where $\boldsymbol{\kappa}^s$ is the symmetric part of $\boldsymbol{\kappa}$ and $\boldsymbol{I}$ is the identity tensor. For simplicity, we have chosen the form appropriate for an infinite aspect ratio [the prefactors differ by $O(1)$ constants for finite aspect ratios [41]]. The coupling $\boldsymbol{F}$ to the flow both induces order and dictates a preferred orientation. The dissipative portion $\boldsymbol{G}$ is

$$\boldsymbol{G}(\phi,\boldsymbol{Q})=6\frac{\overline{D_r}}{k_BT}\frac{v_r}{\phi}\boldsymbol{H}, \tag{3.13}$$

where

$$\overline{D_r}=\frac{\nu_1 D_{r0}}{(1-\frac{3}{2}\,\mathrm{Tr}\,\boldsymbol{Q}^2)^2(cL_0^3)^2} \tag{3.14}$$

is the collective rotational diffusion coefficient and

$$\boldsymbol{H}=-\left[\frac{\delta\mathcal{F}}{\delta\boldsymbol{Q}}-\tfrac{1}{3}\boldsymbol{I}\,\mathrm{Tr}\frac{\delta\mathcal{F}}{\delta\boldsymbol{Q}}\right] \tag{3.15}$$

is the molecular field. D_{r0} is the single-rod rotational diffusion coefficient and ν_1 is an $O(1)$ geometrical prefactor, which will be fixed below Eq. (3.30). The rotational diffusion coefficient is

$$D_{r0}=\frac{k_BT\ln L}{3\pi\eta L_0^3}, \tag{3.16}$$

where η is the solvent viscosity. The $\boldsymbol{Q}$ dependence in the denominator of Eq. (3.14) enhances reorientation for well-ordered systems [40]. Our choice for $\overline{D_r}$ is crude, since it applies to rods in concentrated solution and we use it in the concentrated and semidilute regimes. As with many of our approximations, this gives us a tractable model system with which to study the phenomenology of phase separation.

Doi and co-workers derived Eq. (3.11) for homogeneous systems. We extend this to inhomogeneous systems by including the gradient terms implicit in the functional derivative which defines $\boldsymbol{H}$. Our choice of $\boldsymbol{F}$ is the so-called quadratic closure approximation to the Smoluchowski equation [41]. This approximation ensures that the magnitude of the order parameter remains in the physical range in the limit of strong ordering, but is known to incorrectly predict phenomena such as director tumbling and wagging. Many workers have investigated the subtleties of various closure approximations and the degree to which they reproduce realistic flow behavior [61]. Since our primary goal is to explore the method for calculating phase behavior and outline some of the possibilities for coexistence under flow, we confine ourselves to this well-studied model.

The fluid velocity obeys [40,41,66]

$$\rho(\partial_t+\mathbf{v}\cdot\boldsymbol{\nabla})\mathbf{v}=\boldsymbol{\nabla}\cdot[2\eta\boldsymbol{\kappa}^s+\boldsymbol{\sigma}(\phi,\boldsymbol{\kappa},\boldsymbol{Q})]+\frac{\delta\mathcal{F}}{\delta\phi}\boldsymbol{\nabla}\phi-\boldsymbol{\nabla}p, \tag{3.17}$$

where η is the solvent viscosity, ρ the fluid mass density, and the pressure p enforces incompressibility, $\boldsymbol{\nabla}\cdot\mathbf{v}=\mathbf{0}$. For the low Reynold's number situations considered here, and for steady shear flow, we will equate the left-hand side of the equation above to zero.

The constitutive relation for the stess tensor $\boldsymbol{\sigma}(\phi,\boldsymbol{\kappa},\boldsymbol{Q})$ was derived by Doi and co-workers, and includes dissipative and elastic parts. Since the elastic stress dominates [20], we keep only this part:

$$\boldsymbol{\sigma}\simeq\boldsymbol{\sigma}_{\mathrm{elastic}}=-3\boldsymbol{H}+\boldsymbol{H}\cdot\boldsymbol{Q}-\boldsymbol{Q}\cdot\boldsymbol{H}-\boldsymbol{\nabla}Q_{\alpha\beta}\cdot\frac{\delta\mathcal{F}}{\delta\boldsymbol{\nabla}Q_{\alpha\beta}}. \tag{3.18}$$

The first term of Eq. (3.18) was given by Doi [40], while the last three terms were derived later [5] and are equivalent to the elastic stress due to Frank elasticity [63], generalized to a description in terms of the nematic order parameter $\boldsymbol{Q}$ rather than the nematic director. Note that the last three terms vanish for a homogeneous system.

Finally, the composition equation of motion is of the Cahn-Hilliard form [65],

$$(\partial_t+\mathbf{v}\cdot\boldsymbol{\nabla})\phi=-\boldsymbol{\nabla}\cdot\boldsymbol{J}=\boldsymbol{\nabla}\cdot\boldsymbol{M}\cdot\boldsymbol{\nabla}\mu, \tag{3.19}$$

where $\boldsymbol{M}$ is the mobility tensor and the chemical potential is given by

$$\mu=\frac{\delta\mathcal{F}}{\delta\phi}. \tag{3.20}$$

The diffusive current is $\boldsymbol{J}=-\boldsymbol{M}\cdot\boldsymbol{\nabla}\mu$. The complete dynamics is thus described by Eqs. (3.11), (3.17), and (3.19).

The dynamical equations of motion for other complex fluids have the same theoretical structure: equations of motion for the conserved quantities and the broken-symmetry or flow-induced structural order parameter (analogous to $\boldsymbol{Q}$), and a constitutive relation for the stress as a function of composition and order parameter [66]. For a given system and set of equations of motion, the analysis below is generic. For some local models, internal dynamics [Eq. (3.11)] can be eliminated to give the stress as a history integral over the strain rate. In polymer melts [20] and in wormlike micelles [23] far from a nematic regime, this leads to nonmonotonic stress–strain-rate curves. However, augmenting these integral theories with nonlocal terms to calculate interface profiles is nontrivial.

B. Steady-state conditions

In this work we study planar shear flow, specified by

$$\frac{\partial v_x(\mathbf{r})}{\partial y}=\dot{\gamma}(\mathbf{r}). \tag{3.21}$$

For homogeneous flows $\mathbf{v}(\mathbf{r})=\dot{\gamma} y \hat{\mathbf{x}}$. The phase diagram is given by the domains of stable steady-state solutions to the equations of motion for applied shear stress or strain rate, in the phase space spanned by

$$(\phi, \sigma_{xy}) \quad \text{(common stress)}, \tag{3.22}$$

$$(\phi, \dot{\gamma}) \quad \text{(common strain rate)}. \tag{3.23}$$

For phase separation at common stress, the stress is uniform and the strain rate partitions between the two phases; while for phase separation at common strain rate, the strain rate is uniform and the shear stress partitions between the two phases.

The strain rate tensor is given by

$$\boldsymbol{\kappa}=\dot{\gamma}\begin{pmatrix} 0 & 1 & 0 \\ 0 & 0 & 0 \\ 0 & 0 & 0 \end{pmatrix}. \tag{3.24}$$

Upon rescaling,

$$\hat{\dot{\gamma}}=\frac{\dot{\gamma} L^2}{6 D_{r0} \nu_1 \nu_2^2}, \tag{3.25}$$

$$\hat{\boldsymbol{\sigma}}=\frac{\sigma \nu_2 L^3}{3 k_B T}, \tag{3.26}$$

the steady-state condition for the order parameter [Eq. (3.11)] is

$$0=\frac{1}{u^2 L^2 (1-\frac{3}{2}\mathrm{Tr}\,\boldsymbol{Q}^2)^2}\hat{\boldsymbol{H}}+\hat{\dot{\gamma}}\,\hat{\boldsymbol{F}}, \tag{3.27}$$

where $\boldsymbol{F}=\dot{\gamma}\hat{\boldsymbol{F}}$ and

$$-\hat{\boldsymbol{H}}=\left(1-\frac{u}{3}\right)\boldsymbol{Q}-u\left(\boldsymbol{Q}^2-\frac{\boldsymbol{I}}{3}\mathrm{Tr}\,\boldsymbol{Q}^2\right)+u\boldsymbol{Q}\,\mathrm{Tr}\,\boldsymbol{Q}^2-K\nabla^2\boldsymbol{Q}. \tag{3.28}$$

In steady-state planar shear flow, the velocity gradients are normal to the flow direction, so the convective derivative vanishes and Eq. (3.27) specifies the order parameter in a homogeneous flow. Under these conditions, integration of the momentum equation (3.17) gives a constant stress,

$$\boldsymbol{\sigma}_0=\boldsymbol{\sigma}-p\,\boldsymbol{I}+2\,\eta\boldsymbol{\kappa}^s, \tag{3.29}$$

where $\boldsymbol{\sigma}_0$ is the boundary stress. The rescaled shear stress is

$$\hat{\sigma}^0_{xy}=A\hat{\dot{\gamma}}-uL[\hat{\boldsymbol{H}}+K(\nabla^2\boldsymbol{Q}\cdot\boldsymbol{Q}-\boldsymbol{Q}\cdot\nabla^2\boldsymbol{Q})]_{xy}, \tag{3.30}$$

where $A=2\nu_1\nu_2^3(\ln L)/(3\pi)$ is a constant of order unity: we take $A=1$ for the remainder of this work, which corresponds to a particular choice for ν_1. As with the assumptions of molecular geometry embodied in ν_2 and α [Eqs. (3.7) and (3.8)], different values for A should not qualitatively change the nature of our results.

Integrating the steady-state composition equation (3.19) and using the boundary condition that material cannot enter or leave the system, we find

$$\mu_0=\mu(\mathbf{r}), \tag{3.31}$$

$$\frac{\mu(\mathbf{r})}{k_B T}=F_{\mathrm{Doi}}+\frac{\partial}{\partial\phi}[\phi\ln\phi+L(1-\phi)\ln(1-\phi)]+\phi L\frac{\partial}{\partial u}F_{\mathrm{Doi}}+\tfrac{1}{2}K(\nabla\boldsymbol{Q})^2-gL\nabla^2\phi, \tag{3.32}$$

where Eqs. (3.7) and (3.8) have been used to specify the molecular geometry, μ_0 is a constant of integration, and

$$F_{\mathrm{Doi}}=\tfrac{1}{2}(1-\tfrac{1}{3}u)\mathrm{Tr}\,\boldsymbol{Q}^2-\tfrac{1}{3}u\,\mathrm{Tr}\,\boldsymbol{Q}^3+\tfrac{1}{4}u(\mathrm{Tr}\,\boldsymbol{Q}^2)^2. \tag{3.33}$$

Note that the mobility tensor $\boldsymbol{M}$ plays no role in the steady-state conditions, or in the resulting phase diagram.

Eqs. (3.27), (3.30), and (3.31) completely specify the system in planar shear. Solving these equations will occupy the remainder of this work. Note that variables $\hat{\dot{\gamma}}, \hat{\boldsymbol{\sigma}}, \mu/k_B T$ are all dimensionless quantities.

IV. CALCULATION OF PHASE DIAGRAMS

A. Interface calculation

The phase diagram is specified by solving Eqs. (3.27), (3.30), and (3.31) for given μ_0 and boundary stress σ^0_{xy}. Nonequilibrium ''phases'' are defined as the stable steady-state space-uniform solutions to these equations. These *inhomogeneous* equations comprise a set of ordinary differential equations, through the gradients that appear in the stress and in the functional derivatives that define μ and $\boldsymbol{H}$. The only parameters of the theory are the rod aspect ratio L and the ratio of elastic constants,

$$\lambda=\frac{gL}{K} \tag{4.1}$$

(K may be absorbed into the length scale of the system).

We first fix ϕ (i.e., u) and solve the homogeneous algebraic versions of Eqs. (3.27) and (3.30) for $\boldsymbol{Q}$ and $\dot{\gamma}$ as a function of σ^0_{xy}. In the few cases where the phase diagram in the σ_{xy}-μ plane has a transition line parallel to the μ axis, one must first fix μ_0, and then determine σ_0. This is done for all ϕ. Because $\mathcal{F}(\phi,\boldsymbol{Q})$ describes an I-N transition, at a given stress, multiple roots exist with distinct strain rates and $\boldsymbol{Q}$. Figure 3 shows the stress strain-rate relations for homogeneous solutions to Eqs. (3.27) and (3.30) for $L=5.0$ and $\lambda=1.0$.

The isotropic branch has a larger viscosity than the nematic branch, and has an increasing effective viscosity for increasing concentration, reflecting the contribution $u\hat{\boldsymbol{H}}$ in Eq. (3.30). Conversely, the nematic branch has a lower stress at higher concentrations due to the increased nematic order, which permits less-hindered motion.

For a dilute isotropic system (curve a), shear flow continuously induces nematic order. A more aligned system has a lower effective viscosity, so the stress $\sigma(\dot{\gamma})$ increases slower than linearly (shear thins) as the magnitude of the order parameter $\boldsymbol{Q}$ increases. Eventually the system attains,

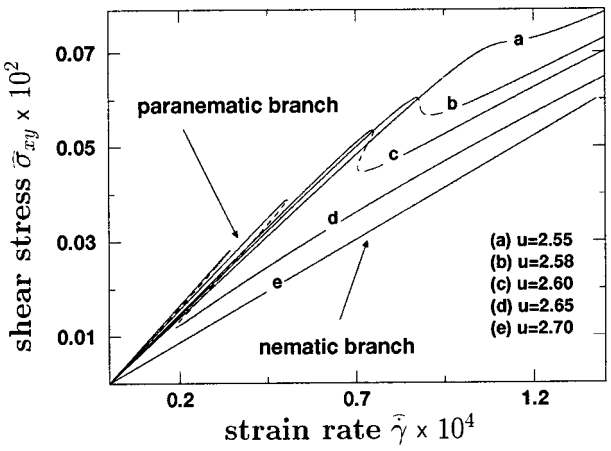

FIG. 3. Homogeneous stress $\hat{\sigma}_{xy}$ vs strain rate $\hat{\dot{\gamma}}$ behavior for various excluded volumes, $L=5.0$ and $\lambda=1.0$. Dotted lines mark unstable branches. Similarly, curves along which $\partial\mu/\partial\phi<0$ are linearly unstable.

smoothly, a high strain-rate state with a much lower viscosity than in the limit of zero stress. For more concentrated systems (curves b, c, and d), shear flow induces a transition to a nematic phase with lower viscosity, and $\sigma(\dot{\gamma})$ is nonmonotonic. There is a region of stresses for which two stable strain rates exist, on either the nematic or isotropic branches of the constitutive curve. For compositions inside the biphasic regime (curve e), both nematic and isotropic branches exist in the limit of zero stress, with the isotropic branch losing stability at high enough stress. Finally (not shown) for highly concentrated systems only nematic branches exist.

As mentioned in Sec. II B, we calculate the phase diagram by explicitly constructing the coexisting interfacial solution [6]. In common stress coexistence, for example, the coexisting states have *different* strain rates and, generally, different compositions. Hence, they connect the high and low strain-rate branches of two different curves in Fig. 3. It is easiest to visualize this by considering the intersection of a plane at a given stress σ^0_{xy} with the surface $\sigma_{xy}(\dot{\gamma},u)$, as in Fig. 4.

At a given stress, the strain rate varies with composition as shown in Fig. 5(a). At coexistence, the chemical potential $\mu(\mathbf{r})$ must be constant through the interface, as dictated by Eq. (3.31). The functional form of the nonequilibrium chemical potential is known from Eq. (3.32), and depends on the strain rate through the dependence of the nematic order parameter on the strain rate in steady state. We plot $\mu(u)$ in

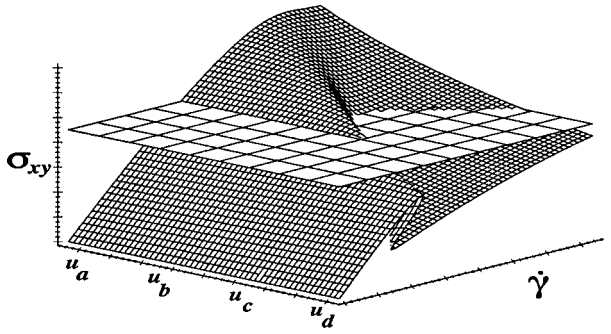

FIG. 4. Stress-strain-composition surface for the curves in Fig. 3. The plane is at $\hat{\sigma}^0_{xy}=0.05$.

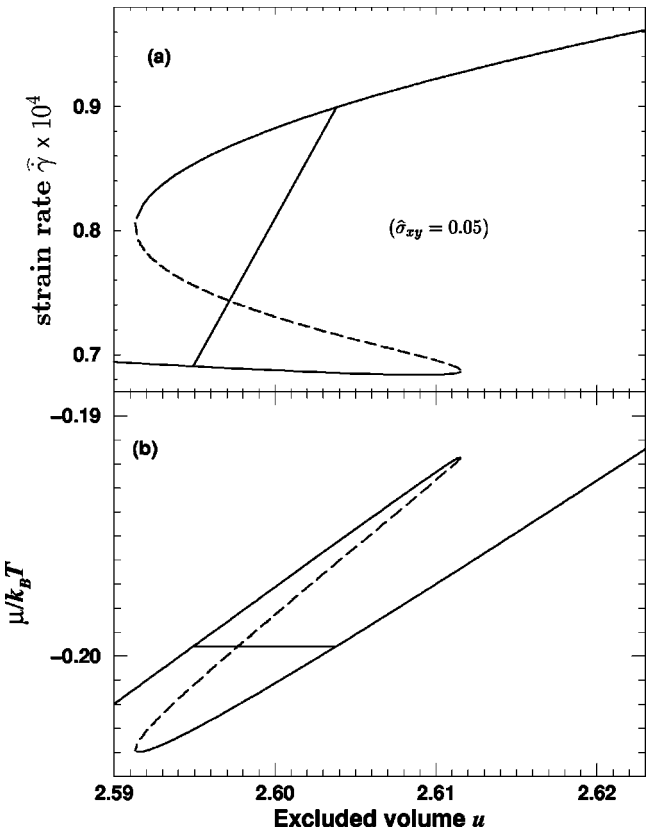

FIG. 5. (a) Reduced strain rate $\hat{\dot{\gamma}}(u)$ and (b) chemical potential $\mu(u)$ for the stress contour in Fig. 4 ($\hat{\sigma}_{xy}=0.05$). The tie line is calculated using the interface construction.

Fig. 5(b). There is a continuum range of μ, which allows possible coexisting pairs of states. (Recall that u is proportional to the rod volume fraction ϕ.)

We now impose the interface solvability condition as follows. For a given stress σ^0_{xy}, we determine a specific coexistence chemical potential μ_0, which allows a stable interfacial solution to Eqs. (3.27), (3.30), and (3.31). In practice, we eliminate $\dot{\gamma}(\mathbf{r})$ from Eq. (3.27) using Eq. (3.30), and solve Eqs. (3.27) and (3.31) for the interfacial profile, with boundary conditions (fixed $\boldsymbol{Q}$ and u) chosen by two points on the low and high strain-rate branches of Fig. 5(b) with the same μ_0. We adjust μ_0 until a stationary interfacial profile is found. This solvability criterion gives sharp selection on μ, and in this way determines a tie line on the $\dot{\gamma}$-u plane, Fig. 5(a). By varying the stress, we compute the entire phase diagram in the σ_{xy}-u and $\dot{\gamma}$-u planes.

For phase separation at a common strain rate, the construction is analogous. One slices a vertical plane through Fig. 4 at a given strain rate, constructs the curve $\mu(u)$ along the intersection with the surface, and searches for a stationary interfacial solution.

The interface calculations are carried out by discretizing the system on a one-dimensional mesh and, from smooth initial conditions, evolving Eqs. (3.27), (3.30), and (3.31) forward using fictitious dynamics calculated with an implicit Crank-Nicholson scheme. Spatial variations are only allowed in the direction in which phase separation occurs, so we replace

$$\nabla \rightarrow \begin{cases} \dfrac{\partial}{\partial y} & \text{common stress} \\ \dfrac{\partial}{\partial z} & \text{common strain rate,} \end{cases} \tag{4.2}$$

where z is in the vorticity direction. We fix the values of u and $\boldsymbol{Q}$ at either side of the interface to lie on the high and low strain-rate branches of Fig. 5, begin with smooth initial conditions, and let the system ''evolve'' towards steady state. An interface develops between the two phases, and moves to one boundary or the other. For a given stress, coexistence is determined by that chemical potential μ for which a stationary interface lies in the interior of the system (in the limit of large system size) [6]. An analogous construction may be made by maintaining a fixed mean strain rate on the unstable part of a homogeneous curve, and then starting up the system and allowing it to select a stress and chemical potential. In either case the selected stress is that stress for which a stationary interfacial solution between the high and low strain-rate branches *exists*. Such an interfacial solution is known in dynamical systems theory as a heteroclinic orbit [59,60,9], and further work will investigate this in more detail for simpler model systems [35,32,67].

We restrict the nematic order parameter to

$$\boldsymbol{Q}=\begin{pmatrix} q_1 & q_3 & 0 \\ q_3 & q_2 & 0 \\ 0 & 0 & -(q_1+q_2) \end{pmatrix}, \tag{4.3}$$

since all steady-state solutions with nonzero elements Q_{xz} or Q_{yz} are unstable due to the symmetry of shear flow [39]. In a similar calculation for thermotropic nematics in shear flow, we have found that this restriction on $\boldsymbol{Q}$ reproduces the same selected stress as that obtained when keeping the full tensor [6].

For planar shear flow and a wide class of equations of motion, we have shown that if a coexisting solution exists, it occurs at discrete points in the parameter set [35]. For example, for a given stress σ_{xy}^0, coexistence can occur only at discrete values for μ_0, that is, along lines in the field variable space spanned by σ_{xy}-μ. This is analogous to equilibrium systems where, for example, phase transitions in a simple fluid occur along lines, rather than within regions, in the pressure-temperature plane.

Note that a one-dimensional calculation does not determine the stability of the interfacial solution with respect to transverse undulations (capillary waves), which could be important in, particularly, the common stress geometry [68].

B. Homogeneous solutions

The modified Doi model in the quadratic closure approximation has three stable solutions in homogeneous planar shear flow. We refer the reader to Bhave *et al.* for further details [39].

(i) I *Paranematic*. The paranematic state I induced from a disordered equilibrium phase. The order parameter $\boldsymbol{Q}$ is small and fairly biaxial, with major axis lying in the shear plane at an angle of almost $\pi/4$ relative to the flow direction.

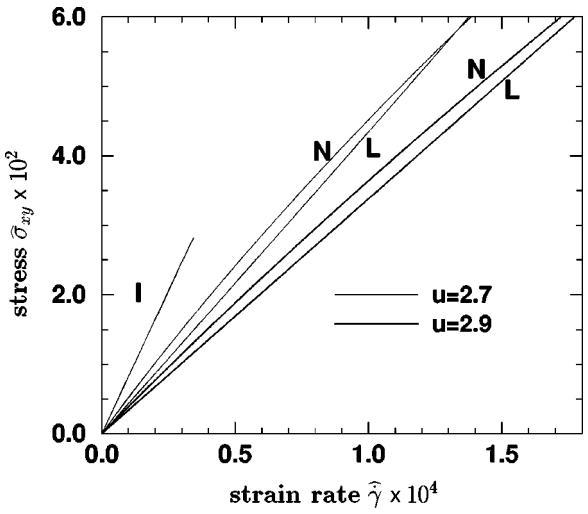

FIG. 6. Constitutive relations for I, N, and L states, for $L=5.0$ and two values for the excluded volume parameter.

(ii) N *Flow-aligning nematic*. The flow-aligning nematic state is much more strongly aligned, has slight biaxiality induced by the flow, and has the major axis of alignment in the flow plane at an angle of a few degrees relative to the flow direction. The I and N states have the same symmetry.

(iii) L *Log-rolling nematic*. The log-rolling phase is also a well-aligned and almost uniaxial phase, but with major axis of alignment in the vorticity ($\hat{\mathbf{z}}$) direction, so the rods spin about their major axes.

The I phase is stable at lower volume fractions and merges with the N phase at high strain rates. The L phase is stable only at higher volume fractions, and is destabilized at high enough strain rates. For low strain rates the stress of the L state is lower than that of the N state, which is lower than that of the I state (see Fig. 6).

Figure 7 shows the regions of stability of the various states. The loop in Fig. 7(a) occurs for compositions such that the constitutive curve $\sigma(\dot{\gamma})$ has the shape of curve b in Fig. 3. Similar phase-plane plots were calculated by Bhave *et al.* [39] and See *et al.* [8]. They did not consider the mixing entropy needed to generate a realistic nematic transition, however, and always generated solutions for a given strain rate instead of a given stress (this explains the absence of a loop in their phase-plane plot $\dot{\gamma}$-ϕ). Their plots (compare Fig. 5 of Ref. [39]) correspond to truncating the loop in Fig. 7(a). Figure 7(b) has a similar, barely discernable, loop near the critical point, within which there are no stable states. This instability is due to the instability of the composition equation, Eq. (3.19). In this region

$$\left.\frac{\partial \mu}{\partial \phi}\right|_{\sigma_{xy}} < 0, \tag{4.4}$$

which is equivalent to a negative diffusion coefficient, and is analogous to the conventional definition of the spinodal line for ordinary equilibrium demixing.

V. COMMON STRESS COEXISTENCE

For common stress coexistence the interface lies in the velocity-vorticity plane, and inhomogeneities are in the $\hat{\mathbf{y}}$

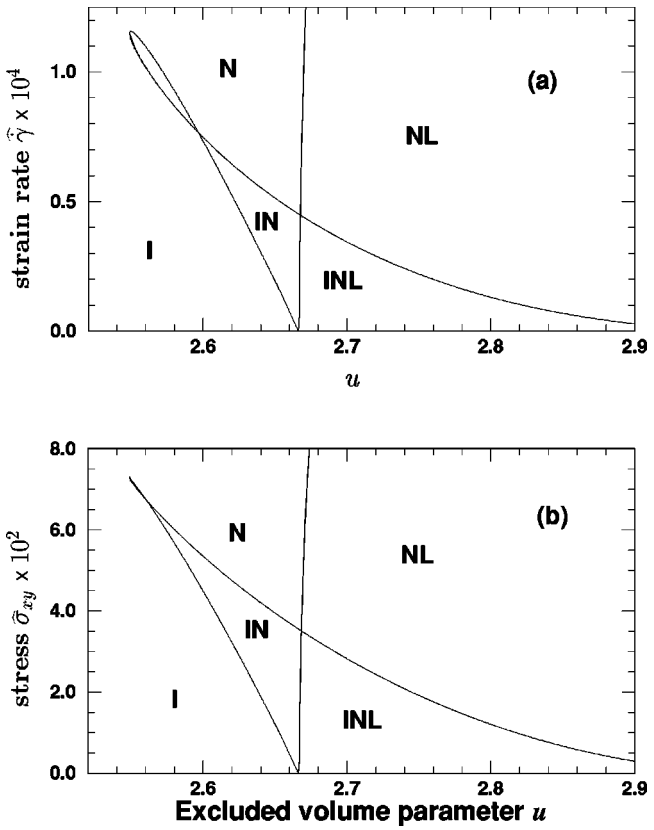

FIG. 7. Regions of stability of paranematic (I), nematic (N), and log-rolling (L) states in the strain-rate–composition (a) and stress-composition (b) planes for $L=5.0$. Note that the loop in (a) contains *no* stable states. Stability limits are calculated with respect to both order parameter and composition fluctuations, for a given controlled stress. The thin loop in (b) encloses a region with no stable states, due to the instability of the composition equation.

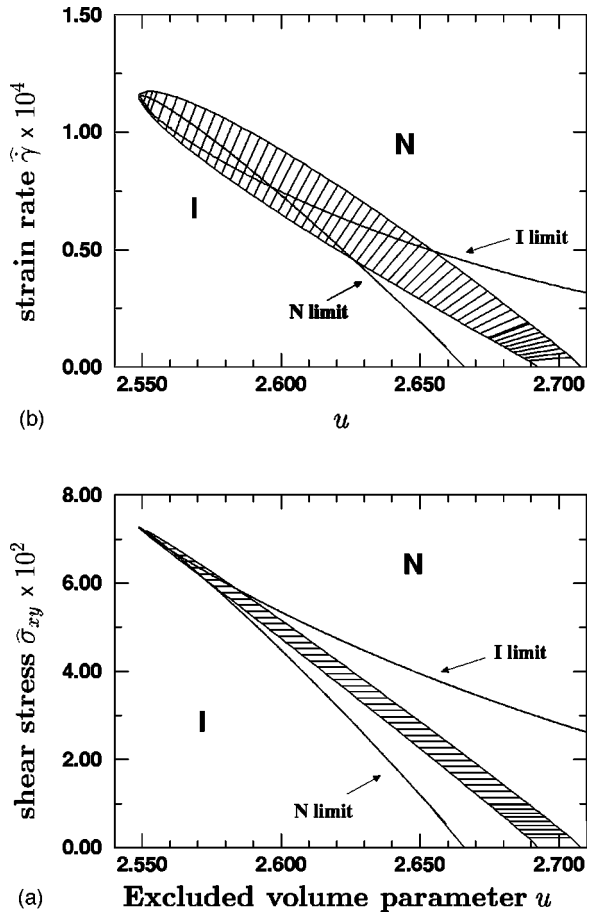

FIG. 8. Phase diagram in the $(\hat{\sigma}_{xy}\text{-}u)$ (a) and $(\hat{\dot{\gamma}}\text{-}u)$ (b) planes for $L=5.0$, $\lambda=1.0$, along with the limits of stability of I and N phases.

direction (see Fig. 2). The stress balance condition at the interface is $\boldsymbol{\sigma}\cdot\hat{\mathbf{y}}$ uniform. σ_{yy} is taken care of by the pressure and σ_{zy} vanishes by symmetry (no flow in the $\hat{\mathbf{z}}$ direction), leaving continuity of the shear stress σ_{xy} through the interface. The two coexisting phases *I* and *II* have strain rates and compositions partitioned according to

$$\overline{\phi}=\zeta\phi_I+(1-\zeta)\phi_{II}, \tag{5.1}$$

$$\overline{\dot{\gamma}}=\zeta\dot{\gamma}_I+(1-\zeta)\dot{\gamma}_{II}, \tag{5.2}$$

where $\overline{\phi}$ and $\overline{\dot{\gamma}}$ are the mean composition and strain rate and ζ is the fraction of material in phase *I*.

A. Paranematic–flow aligning coexistence (I-N)

Phase diagram. Figure 8 shows the tie lines computed on the $(\hat{\sigma}_{xy}\text{-}u)$ and $(\hat{\dot{\gamma}}\text{-}u)$ planes according to the procedure outlined in Sec. III. Several features should be noted. Flow induces nematic behavior in what, in equilibrium, would be an isotropic phase. The tie lines are horizontal in the $(\hat{\sigma}_{xy}\text{-}u)$ plane, since phases coexist at a prescribed stress, and have a positive slope in the $(\hat{\dot{\gamma}}\text{-}u)$ plane because the more concentrated nematic phase flows faster. There is a critical point at sufficiently strong stress, whose existence is expected since the flow-aligning nematic and paranematic states have the same symmetry ($\boldsymbol{Q}$ is biaxial) and their major axes are in the shear plane.

More interesting is the changing slope of the tie lines. For weak stresses the equilibrium system is slightly perturbed and the tie lines are almost horizontal. For high stresses the tie lines become more vertical and the composition difference between the phases decreases. The slope of the tie lines determines the shape of the mean stress–strain-rate relation $\overline{\sigma}_{xy}(\overline{\dot{\gamma}})$ that would be measured in steady-state experiments.

Mean constitutive relations. Consider a composition in the range where phase separation occurs. For small applied stress $\overline{\sigma}_{xy}(\overline{\dot{\gamma}})$ varies smoothly until the two-phase region is reached. At this stress, a tiny band of high strain-rate strongly aligned nematic material appears, with volume fraction determined by the lever rule, Eq. (5.1). The mean strain rate $\overline{\dot{\gamma}}$ is determined by the lever rule, Eq. (5.2), and the measured constitutive relation $\overline{\sigma}_{xy}(\overline{\dot{\gamma}})$ is nonanalytic at this point (see Fig. 9). As the stress is increased further, the system traverses the two-phase region by jumping from tie line to tie line. Each successive tie line has a higher stress, a higher mean strain rate, and a steadily increasing volume fraction of nematic phase. The compositions of both coexisting phases change steadily through the two-phase region.

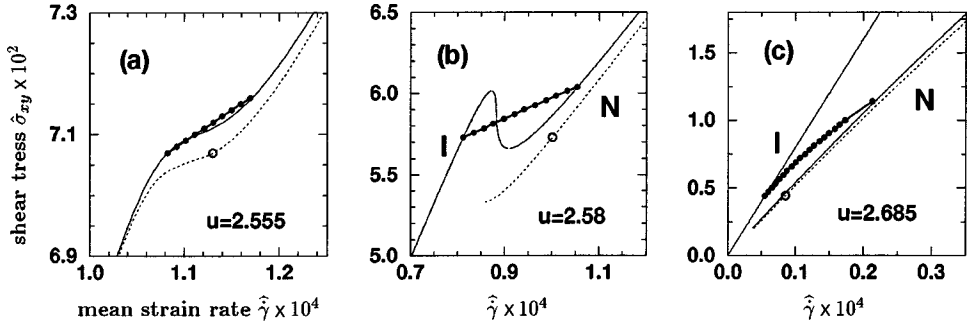

FIG. 9. Mean stress–strain-rate curves for coexistence at common stress, for $L=5.0$ and $\lambda=1.0$. The solid lines denote I and N branches; the dotted line in each figure denotes the stable N branch with which the I state coexists at the low strain-rate boundary of the coexistence region, at a strain rate marked by an open circle ○. The solid circles ● and thick solid line denote the stress that would be measured in the banded regime. Phase coexistence occurs between phases of *different* compositions than the mean compositions ($u=2.555,\ 2.58,\ 2.685$). The unstable portion of the homogeneous flow curve is shown in (a) and (b), but not (c). Note that the plateaus in the two-phase regions in (a) and (b) rather obviously do *not* satisfy an equal area construction with the underlying constitutive curve at the mean composition.

The constitutive relation $\overline{\sigma}_{xy}(\overline{\dot{\gamma}})$ through the two phase region is determined by the spacing and splay of the tie lines. For mean compositions $\overline{\phi}$ close to the equilibrium isotropic-nematic transition [Fig. 9(c)], the tie lines in the ($\hat{\dot{\gamma}}$-u) plane are fairly flat, so that the stress σ_{xy} changes significantly through the two-phase region, and the ''plateau'' has definite curvature, reflecting the initial splay of the tie lines. For slightly lower mean compositions [Fig. 9(b)] the ''plateau'' is straighter and flatter, as can be seen in (Fig. 10), because the lines are more vertical in the ($\hat{\dot{\gamma}}$-u) plane. Finally, for compositions near the critical point the plateau is flatter still but, more interestingly, phase coexistence occurs in a region where the stress-strain curve at the mean composition is no longer nonmonotonic [Fig. 9(a)]. This is because stability in a two-phase system is also determined by the stability with respect to composition variations. In fact, the local chemical potential $\mu(u)$ has negative slope and is unstable on a segment of this curve. The tie line construction is a graphical expression of the explanation proposed by Schmitt *et al.* [28], who attributed a sloped plateau to composition dependence of the stress-strain constitutive relation. The general relation is given by

$$\frac{\partial\sigma}{\partial\overline{\dot{\gamma}}}=\left[\frac{\zeta}{\eta_I}+\frac{1-\zeta}{\eta_N}-m(\sigma)\left\{\frac{1-\zeta}{\dot{\gamma}_N'\eta_N}+\frac{\zeta}{\dot{\gamma}_I'\eta_I}\right\}\right]^{-1}, \quad (5.3)$$

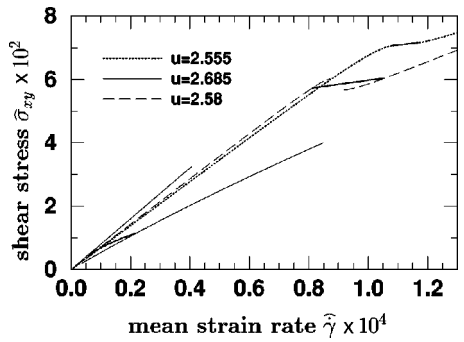

FIG. 10. $\hat{\sigma}_{xy}$ vs $\hat{\dot{\gamma}}$ for common stress coexistence for $L=5.0$ and $\lambda=1.0$. The solid lines connecting the high and low strain rate branches at each composition denote the composite flow behavior at coexistence.

where $m(\sigma)$ is the slope of a tie line with stress value σ, the lines $\{\sigma_I(\phi),\sigma_N(\phi),\dot{\gamma}_I(\phi),\dot{\gamma}_N(\phi)\}$ bound the phase-coexistence domains in the σ-ϕ and $\dot{\gamma}$-ϕ planes, $\eta_k=\partial\sigma_k/\partial\dot{\gamma}$ is the local viscosity of the kth branch, and $\dot{\gamma}_k'=\partial\dot{\gamma}_k/\partial\phi$.

Measurements at controlled stress or controlled strain rate. Although these calculations are for phase separation at a common stress, one may perform experiments at either controlled stress or strain rate. All three composite curves in Fig. 9 have similar shapes, so we expect the same qualitative behavior for all compositions. Controlled strain-rate experiments should follow the homogeneous flow curves, except for strain rates in the coexistence regime. Here we expect the steady state to eventually be the banded state. This should presumably occur by a nucleation event after some time, for start-up strain rates less than the I limit shown in Fig. 8(a), and should occur immediately for imposed strain rates beyond this stability limit. Conversely, upon decreasing the strain rate from the nematic phase, we expect nucleated behavior for strain rates larger than the N limit, and instability for smaller strain rates. In the metastable regime we expect the flow curve to follow the underlying homogeneous constitutive curve for the given composition, until the nucleation event occurs. Interestingly, there is a small region [inside the loop in Fig. 8(a)] where the system is unstable when brought, at controlled strain rate, into this region from either the I or N states. This corresponds to constitutive curves with the multivalued behavior of curve b in Fig. 3.

Controlled stress experiments should exhibit similar behavior. Consider Fig. 9(b). For initial applied stresses larger than the minimum coexistence stress and less than the I limit of stability in Fig. 8(b), we expect the system to follow the homogeneous flow curve until a nucleation event occurs. After nucleation, the strain rate should increase, until either the proper plateau strain-rate or the high strain-rate nematic state is reached, depending on the magnitude of the stress. For stresses larger than the limit of stability, we expect the system to become immediately unstable to either a banded flow or a homogeneous nematic phase, depending on the magnitude of the stress.

Metastability: Experiments. Experiments on wormlike micelles [1,2,29] have found constitutive curves analogous to

those in, say, Fig. 9. In these experiments the plateau appears to be the stable states, while the portion of the constitutive curve (a ''spine'') which extends to stresses above the onset of the stress plateau appears to be a metastable branch on which the system may remain for a finite period of time under controlled stress or strain-rate conditions. References. [2,29,51] conducted controlled strain-rate experiments and found that the system follows the composite curves (without ''spines'' that extend above the onset of the stress plateau) in Fig. 9, if care is taken to reach steady state. In these systems the plateaus were nearly flat, suggesting a very slight dependence of the flow behavior on composition. For controlled strain-rate quenches into what corresponds to the two-phase region of Fig. 8(a), the system took some time to develop shear bands and phase separate. This relaxation or ''nucleation'' time decreased as the mean strain rate was increased [29]. It is not clear that they reached a limit of stability (which would be analogous to the I limit in Fig. 8). The relaxation times were of order 60–600 s, depending on temperature, mean composition, and mean strain rate. We emphasize that these experiments were on micellar solutions, which probably do not show an isotropic-nematic transition, but still display the same qualitative stress–strain-rate relationship as curve b in Fig. 3.

Reference [44] revealed different stress plateaus upon controlling either the strain rate or the shear stress (see Fig. 7 of Ref. [44]) in cone-and-plate flow. In controlled stress experiments, the stress plateau occurred at a stress of order 1.5 times the stress plateau observed under controlled strain-rate conditions. Moreover, the flow curve under controlled stress conditions exhibited a stress maximum and then a decrease in stress to an approximate flat plateau. One explanation for the high stress plateau under controlled stress conditions could be that the ''spine'' never nucleated under controlled stress conditions, and the system smoothly transformed to the high strain-rate phase. However, we do not have an explanation for the decrease and subsequent plateau in stress under applied strain-rate conditions.

In other experiments, controlled stress experiments revealed two kinds of metastable behavior [29]. For $\sigma_p < \sigma < \sigma_{\rm jump}$, where σ_p is the minimum stress for the onset of banding in controlled strain-rate experiments, the system maintained a strain rate on the ''metastable'' branch for indefinite times (measured times were up to 10^4 s). For $\sigma > \sigma_{\rm jump}$ the system accelerated, after of order 10^3 s, and left the rheometer. For these systems it is not clear whether a stable high shear branch exists. An explanation for $\sigma_{\rm jump}$ is lacking. Evidently the nucleation processes governing metastability at controlled stress and controlled strain rate are different. Clearly we need more experiments and theory about the nature of nucleation and metastability in controlled stress versus controlled strain-rate experiments.

Polydispersity. Figure 11 shows the effect of rod aspect ratio L on the phase diagram. A smaller rod aspect ratio couples more weakly to the flow, requiring a slightly larger strain rate to induce a transition to the nematic phase [Fig. 11(a)]. The resulting stress is slightly smaller because, when the system enters the two-phase region the stress is largely determined by that of the paranematic branch, which decreases with increasing L [Fig. 11(b)]. Although the equilibrium phase boundaries are close [see Eqs. (3.9) and (3.10)],

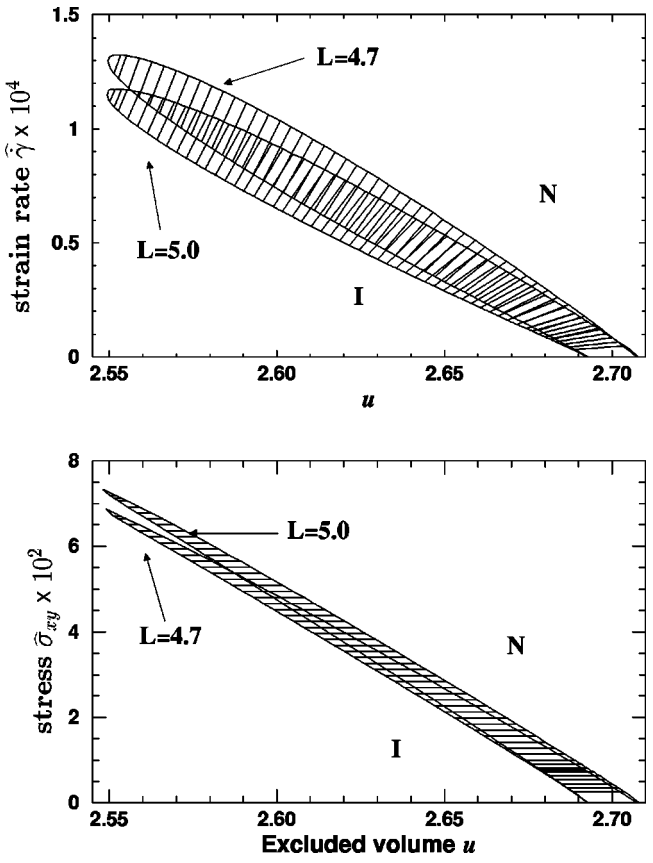

FIG. 11. Phase diagrams for $L=5.0$ and $L=4.7$ at common stress, for $\lambda=1.0$.

the deviation is amplified considerably by applying flow. This suggests that flow enhances the natural tendency of length polydispersity to widen biphasic regimes.

B. Paranematic–log-rolling coexistence (I-L)

Figure 12 shows the phase diagram calculated for coexistence between paranematic (I) and log-rolling (L) states. As with I-N coexistence, the zero shear limit corresponds to the equilibrium biphasic region. However, for nonzero stress the biphasic region shifts in the direction of higher concentration. This is reasonable, since the stability limit of the L phase shifts to higher concentrations with increasing stress (Fig. 7). Note also that, since the I and L phases have major axes of alignment in orthogonal directions, there is no critical point. Instead, the window of phase coexistence ends when the I phase becomes unstable to the N phase.

We have also computed phase coexistence between N and L phases. This occurs at much higher compositions ($u > u_* \gtrsim 3.0$) and has a narrow width in composition due to the very slight difference in viscosities of the two phases. Unfortunately, we cannot resolve this coexistence regime accurately within the numerical precision of our calculations and do not present these results here.

The existence of two possible phase diagrams for common stress phase separation raises an interesting question. Can one observe I-L coexistence? Notice that I-L coexistence can only occur for samples prepared at concentrations at or above that necessary for equilibrium phase separation. One could prepare a phase-separated isotropic-nematic mixture

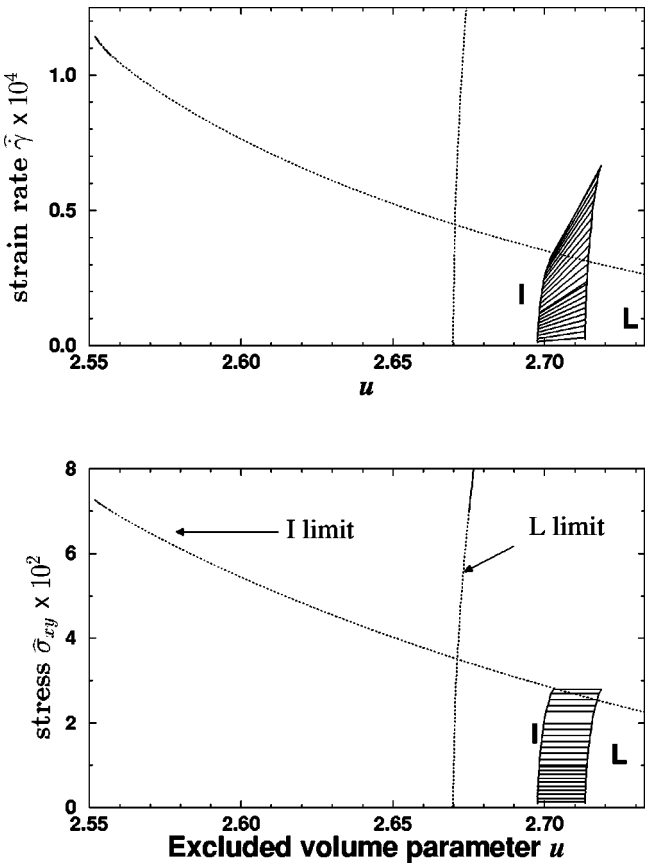

FIG. 12. Phase diagram in the ($\hat{\sigma}_{xy}$-u) and ($\hat{\gamma}$-u) planes for paranematic–log-rolling coexistence, for $L=5.0$ and $\lambda=1.0$. The dotted lines are the limits of stability of the I and L phases (see Fig. 7).

and, by wall preparation, field alignment, sedimentation, or other techniques, separate the phases into two macroscopic domains with the nematic phase in the log-rolling geometry.

Upon applying shear, the system could then maintain coexistence and move through the I-L two-phase region. However, under controlled strain-rate conditions, the I material could decay into I-N coexistence (see Fig. 13). The resulting I-N coexistence would quickly destabilize the entire I-L structure. Therefore, the three-band structure N-I-L will not be present in this model, and it is probable that I-L coexistence could only exist under flow as a metastable state. Similar conclusions may be drawn by examining the phase diagrams in field-variable space, μ-σ_{xy}, as in Fig. 18(a). In this case the chemical potential of the I phase, at I-L coexistence, is within the N region of the phase diagram for I-N coexistence, indicating a (possibly metastable) instability with respect to I-N phase separation. Moreover, the chemical potentials of the three phases are never the same, except at rest where the L and N states are identical apart from the rod orientations.

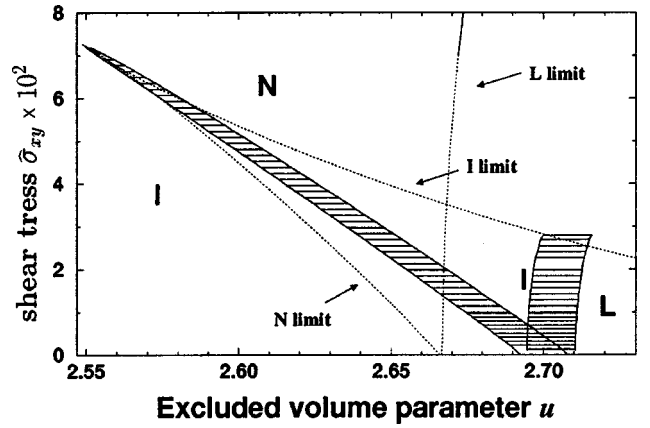

FIG. 13. Composite phase diagrams for I-L and I-N coexistence at common stress for $L=5.0$ and $\lambda=1.0$. We stress that this represents *two* overlayed phase diagrams, and not a single phase diagram. For example, there is *no* triple point implied by the intersection of the I-N and I-L phase diagrams.

VI. COMMON STRAIN-RATE COEXISTENCE

For coexistence at common strain rate the interface lies in the velocity–velocity-gradient plane, and inhomogeneities are in the $\hat{\mathbf{z}}$ direction (see Fig. 2). The stress balance condition at the interface is $\boldsymbol{\sigma}\cdot\hat{\mathbf{z}}$ uniform. As before, σ_{zz} is taken care of by the pressure while σ_{yz} and σ_{xz} are zero by symmetry (and because there are no stable q_3 components in the order parameter tensor). With bands in the $\hat{\mathbf{z}}$ direction, the strain rate in each band is set by the relative velocity of the two plates (or cylinders, in a Couette device), and the shear stresses differ. The mean applied stress $\overline{\sigma_{xy}}$ is the area aver-

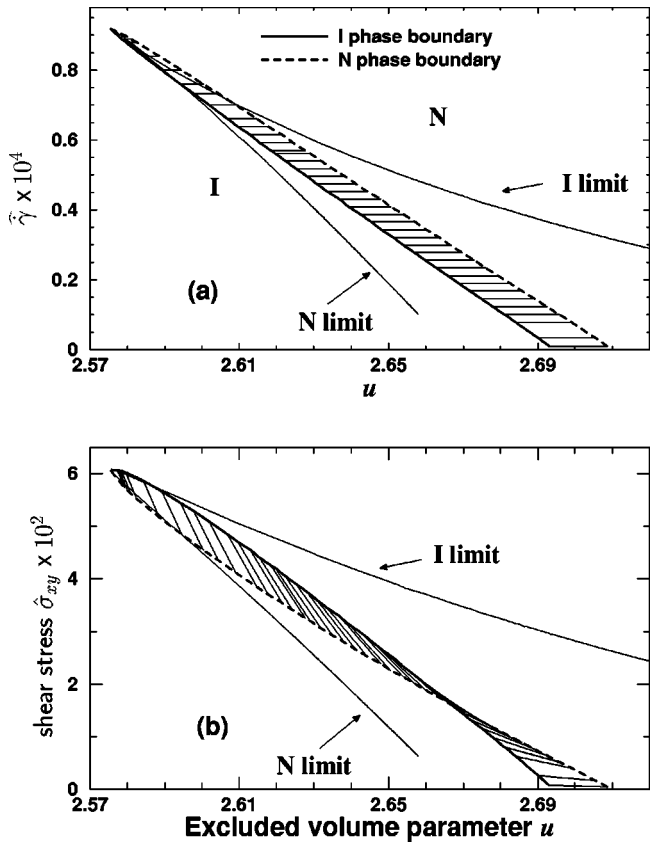

FIG. 14. Common strain-rate phase diagram in the ($\hat{\gamma}$-u) (a) and ($\hat{\sigma}_{xy}$-u) (b) planes, for $L=5.0$ and $\lambda=1.0$. Also shown are the limits of stability of the I and N phases (calculated for a given imposed strain rate, in contrast to Figs. 7, 8, 12, and 13, in which the stability was calculated for an imposed stress).

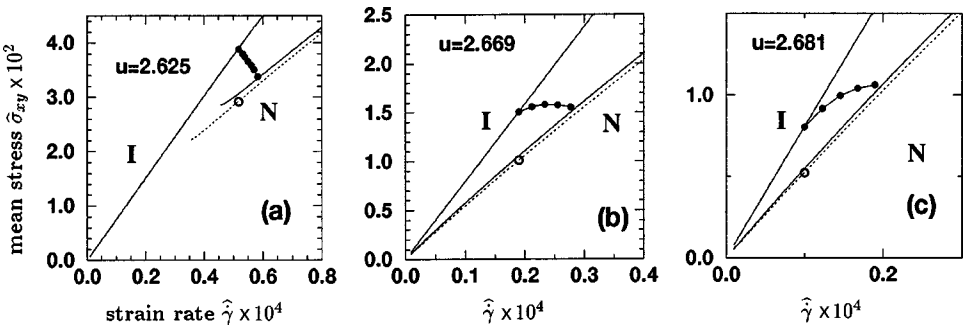

FIG. 15. Mean stress–strain-rate curves for common strain-rate coexistence for $L=5.0$ and $\lambda=1.0$. The solid lines denote the stable I and N branches; the dotted line in each figure denotes the stable N branch with which the I state coexists at the low strain-rate boundary of the coexistence region, at a strain rate marked by an open circle ○. The solid circles ● and thick solid line denote the stress that would be measured in the banded regime. The filled circles ● and thick solid line denotes the stress measured under banded conditions.

age of the stress applied to each band. The coexisting phases have shear stresses and compositions partitioned according to

$$\overline{\phi}=\zeta\phi_I+(1-\zeta)\phi_{II}, \tag{6.1}$$

$$\overline{\sigma}_{xy}=\zeta\sigma^I_{xy}+(1-\zeta)\sigma^{II}_{xy}, \tag{6.2}$$

where $\overline{\sigma}_{xy}$ is the mean shear stress. The interfacial equations to solve are Eqs. (3.27), (3.30), and (3.31).

Phase Diagram. Common strain-rate I-N phase coexistence is shown in Fig. 14. In this case the tie lines are horizontal in the $(\hat{\dot{\gamma}}$-$u)$ plane. They have a negative slope in the $(\hat{\sigma}_{xy}$-$u)$ plane because the paranematic I phase coexists with a denser and less viscous flow-aligning N phase. As with phase separation at common stress, there is a (very small) loop in the limits of stability in the control variable plane $(\dot{\gamma}$-$u)$ within which there are no stable homogeneous states. The careful reader will note that the limits of stability at a given stress (Fig. 8) are different from the limits of stability at a given strain rate. This is physically correct, and will be discussed below in Sec. VII C.

There is an interesting crossover visible in the $(\hat{\sigma}_{xy}$-$u)$ plane. For higher mean compositions the fluid has a higher stress in its high strain-rate one-phase region than in its low strain-rate one-phase region; that is, respectively above and below the biphasic region in the Fig. 14(a). Conversely, for low enough compositions $u\lesssim 2.67$, the stress in the high strain-rate region immediately outside the biphasic regime is actually *less* than the stress just before the system enters the biphasic region, as can be seen by the crossing of the solid and dashed phase boundaries in Fig. 14.

This crossover is straightforward to understand. Since phase separation occurs at a given strain rate, and the stress of the N branch at a given composition and strain rate is always less than that of the corresponding I branch, we expect a decrease in the stress upon leaving the biphasic regime in cases where the coupling to composition is less important. We saw in the analysis at common stress that composition effects are less important (for I-N coexistence) at lower compositions and high strain rates, where the tie lines are more vertical. We expect this near the critical point where the two phases become more and more similar. More generally, we expect this behavior in situations where phase separation occurs at a common strain rate into a shear-thinning state with only slight changes in composition. In the more concentrated regime, the coexistence plateau traverses a wider range of concentrations and strain rates, and emerges into the pure N phase with a higher stress (the width in strain rate of the phase-coexistence regime is enough to overcome the shear thinning effect of the nematic phase).

Mean constitutive relations. Figures 15 and 16 show the mean stress–strain-rate relations. As with common stress phase separation, the shape of the ''plateau'' as the strain rate is swept through the two-phase region is not always flat, and depends on the splay of the tie lines. At higher concentrations the plateau has a positive slope while, in accord with the crossover in the $(\hat{\sigma}_{xy}$-$u)$ phase diagram, for lower concentrations the plateau crosses over to negative slope, which usually signifies a bulk instability. A simple argument, analogous to that for the stability of a bulk fluid, supports this. However, we note that a composite negative slope curve was accessed, and apparently found stable, by Hu *et al.* [69] under controlled stress conditions. The negative slope in Fig. 15(a) is likely to be inaccessible under controlled stress conditions, and the instability argument may apply to controlled strain-rate conditions. The general relation for the slope in the composite region is [28]

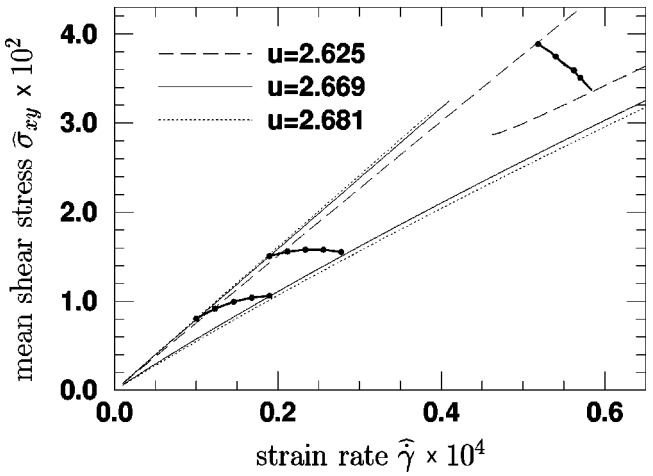

FIG. 16. $\hat{\sigma}_{xy}$ vs $\hat{\dot{\gamma}}$ for various compositions, for phase separation at common strain rate and $L=5$.

$$\frac{\partial\overline{\sigma}}{\partial\dot{\gamma}} = \eta_I\,\zeta + \eta_N(1-\zeta) - m(\dot{\gamma})\left\{\frac{\eta_N(1-\zeta)}{\sigma_N'} + \frac{\eta_I\,\zeta}{\sigma_I'}\right\}, \tag{6.3}$$

where $m(\dot{\gamma})$ is the slope of the tie line with strain rate $\dot{\gamma}$ and $\sigma_k' = \partial\sigma_k/\partial\phi$. In the limit of no concentration difference [$\delta\phi = 0$ or $m(\dot{\gamma}) = \infty$], $\sigma(\dot{\gamma})$ is vertical through the two-phase region.

Measurements at controlled stress or controlled strain rate. For controlled strain-rate measurements we expect behavior similar to that for phase separation at common stress. For start-up experiments with mean strain rates larger than the minimum strain rate for coexistence at a given composition, we expect the stress to follow the metastable branch until a nucleation event causes the stress to decrease to the plateau stress. The exception is a composition such as that in Fig. 15(a), for which the composite flow curve for I-N coexistence may be mechanically unstable. Similar results should apply upon decreasing the strain rate from the shear-induced N phase to below the N limit. As before, this expectation of a nucleation event is based on a possibly misguided analogy with equilibrium systems which, nonetheless, is encouraging given the experiments which see ''nucleation''-type behavior in micelles under flow [2,29,51].

For controlled stress, the situation is slightly different. For compositions with mean stress–strain-rate curves of the shape of Fig. 15(c), we expect similar behavior to that found for common stress phase separation. However, for compositions that yield curves such as Fig. 15(a), there is a window of stresses for which there are *three* possible states: homogeneous low strain-rate and high strain-rate branches, and a banded intermediate branch. We emphasize that we have not determined the absolute stability of any of these branches. A possibility is that the system has hysteretic behavior. For example, in start-up experiments the system would remain on the I branch until a certain stress, at which point it would nucleate after some time and transform to either the high strain-rate N branch or coexistence. We cannot tell which state it might go to, from this analysis, but it seems likely that it would jump straight to the N branch. If the system jumped from the I branch to the coexistence branch, increasing the stress further would *decrease* the strain rate and return the system to the I branch. Since it originally nucleated *from* the I branch, it seems unlikely that the original jump could be to the coexisting plateau. The same behavior (in reverse) would be expected upon reducing the stress from the high strain-rate N phase.

Although there have been anecdotal reports of shear banding in the common strain-rate geometry, there have been very few such results published [13]. Bonn *et al.* [38] have recently reported results for sheared surfactant onion gels, along with visual confirmation of bands in the common strain-rate geometry. In controlled strain-rate experiments they found constitutive curves analogous to Figs. 15(a) or 15(b). In controlled stress experiments they found hysteretic behavior, with the system flipping between high and low strain-rate branches after some delay time, missing the coexistence ''plateau'' regime. However, it is not clear that these were true steady-state results.

Stable ''negative-slope'' behavior was seen in a shear-thickening system which phase separates at common stress [52,53], under controlled stress conditions. In this case there was a single (mean) strain rate for a given applied stress, and the measured constitutive relation had an S shape rather than the sideways S shape of Fig. 15.

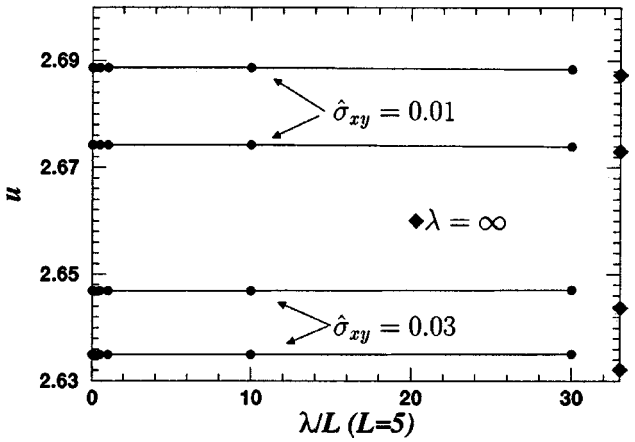

FIG. 17. I-N phase boundaries for common stress phase separation as a function of λ/L, for $L = 5.0$. The diamonds ◆ are for $\lambda = \infty$ ($K = 0, g = 1$).

VII. DISCUSSION

A. Dependence on gradient terms

Gradient terms appear in all equations of motion for $K \neq 0$ and for any g, so to avoid unphysical equations without gradients (which cannot resolve interfaces) we must have $\lambda \sim g/K < \infty$. In the case of $K = 0$ and finite g, the $\boldsymbol{Q}$ equation of motion has no explicit gradient terms and hence can, in principle, support discontinuous solutions. The ϕ equation has gradients in this case, arising from the term $g(\nabla\phi)^2$ in the free energy density, Eq. (3.2), so the system will eventually reach a state with smooth solutions in both ϕ and $\boldsymbol{Q}$. Conversely, for $g = 0$ there are gradient terms in both the $\boldsymbol{Q}$ and ϕ dynamics, with the latter arising from the term $\phi(\nabla\boldsymbol{Q})^2$ in the free-energy density Eq. (3.2).

Phase boundaries for $\hat{\sigma}_{xy} = 0.01,\ 0.03$ are shown in Fig. 17. For $\lambda \in (0.0\text{–}30.0)$ the phase boundaries are the same, within the precision of our numerical calculations, while there is a distinct difference for $\lambda = \infty$. We have discretized the system on a mesh of 125 points, and the range of elastic constants is such that the width of the interface is at least 20 mesh points, large enough for smooth behavior and much smaller than the system size.

We cannot rule out the possibility that changes in λ shift the phase boundaries by small amounts below our accuracy, which is of order 0.1% in u, but the apparent independence of the phase boundaries on λ is curious. One might be tempted to generalize and suggest that, for finite λ, there exists a selection criterion which involves only the homogeneous equations of motion, rather than requiring the inhomogenous terms as in the interface construction. An interface construction may also be used to determine equilibrium phase boundaries, in which case a stationary interface is equivalent to minimizing a free energy and the (relaxational) dynamical equations derived from a variational principle [6].

In the case of a van der Waals fluid this reproduces the Maxwell construction.

A steady state equation for a single variable ψ with homogeneous and inhomogeneous terms of the form

$$\sigma_0 = f_{\rm hom}(\psi) + f_{\rm inh}(\partial\psi/\partial y) \tag{7.1}$$

can be integrated to yield a solvability condition for σ_0, which is equivalent to the stable interface method. In equilibrium $f_{\rm inh}$ integrates exactly without an integrating factor, since it typically arises from a variation of a free-energy functional with respect to ψ, and the result σ_0 (corresponding to the pressure in the van der Waals fluid) depends only on $f_{\rm hom}$. Out of equilibrium, integration is not so simple, and the solvability condition depends, generally, on the form of the gradient terms [60,35].

In the multivariable case considered here, the steady-state conditions for the order parameter and composition are coupled differential equations which are not integrable in shear flow. This is because of the terms $\boldsymbol{\kappa}\cdot\boldsymbol{Q}+\boldsymbol{Q}\cdot\boldsymbol{\kappa}^T$ in Eq. (3.12) and $(\nabla^2\boldsymbol{Q})\cdot\boldsymbol{Q}-\boldsymbol{Q}\cdot(\nabla^2\boldsymbol{Q})$ in Eq. (3.30). In extensional flow $\boldsymbol{\kappa}$ is symmetric, so that $\boldsymbol{\kappa}\cdot\boldsymbol{Q}+\boldsymbol{Q}\cdot\boldsymbol{\kappa}^T$ integrates to $\mathrm{Tr}(Q^2\boldsymbol{\kappa})/2$, while in shear flow this term can only be integrated by introducing an integral representation [70]. Hence a first integral of the steady-state equations cannot be found in shear flow, and it seems unlikely that a general condition involving only the homogeneous portion of the steady-state equations can determine coexistence. While we appear to find, for this set of gradient terms, solvability conditions that are independent of λ for $\lambda<\infty$, the relationship of this to a variational principle remains unknown. We have not exhausted the possible gradient terms. For example, higher-order gradients in the free energy $[(\nabla^2\boldsymbol{Q})^2$, etc.] would yield higher-order differential equations for the interfacial profile, and other square gradient terms such as $Q_{\alpha\beta}\nabla_\alpha\nabla_\beta\phi$ are possible [71]. Hence, we believe that, for finite λ, *the apparent independence of our results on gradient terms only applies to the particular (simple) family of gradient terms we have chosen*. The structure of the differential equations describing the steady states may change abruptly for $\lambda=\infty$, for which a term is lost in the differential equations, leading to a distinctly different selection criteria and the shifted phase boundary in Fig. 17. Unfortunately, this particular set of equations is too complex for this kind of analysis. For example, in a study of a simpler constitutive model, one can demonstrate that the selected stress depends on the detailed form of the gradient terms [35].

Several workers have claimed to find an equal-area construction on the stress–strain-rate constitutive curve [30]. That is, the ''plateau'' as the system traverses the two-phase region is said to describe a path such that the areas above and below the plateau, enclosed by the plateau line and the underlying constitutive curve, are the same. This is not true here, as can be seen in Fig. 15.

B. Which phase separation is preferred?

Having calculated *both* common strain rate and common stress phase separation for the same system, and noticing from Figs. 13 and 14 that there are compositions and shear conditions which lie inside the two-phase regions of all three calculated phase separations, we must address the question

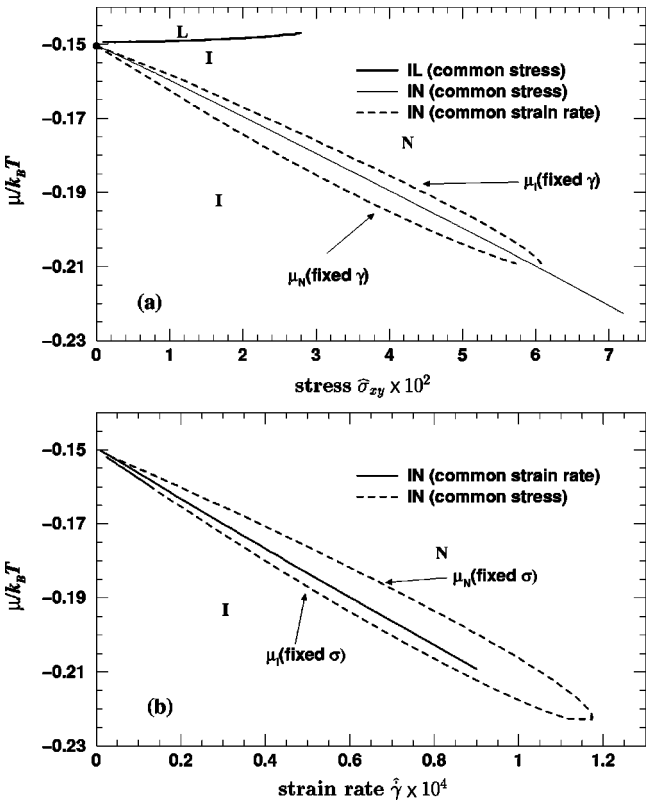

FIG. 18. Phase diagrams in the chemical potential μ vs stress plane (a) and the μ–strain-rate plane (b). The solid lines denote the phase boundaries for common stress phase coexistence in the μ-σ_{xy} plane (a) and for common strain-rate coexistence in the μ-$\dot\gamma$ plane (b). The dashed lines denote the coexisting stresses for common strain-rate phase separation within the common stress phase diagram (a), and vice versa in (b).

of which phase separation occurs. We have already argued that we expect I-L phase separation at common stress to be metastable with respect to I-N phase separation at common stress. What about the relative stability of I-N phase separation at either common stress or common strain rate?

With limited one-dimensonal calculations for systems of different symmetry (annular bands at common stress and stacked disklike bands for common strain rate), it is impossible to calculate the stability of one interface profile with respect to another. Renardy calculated the stability of common stress coexistence to capillary fluctuations [68], which is a start, and such a stability analysis has been performed, in part, on the layer orientation of smectic systems in flow [16]. However, some insight can be obtained by examining the ''phase diagrams'' in the chemical potential-field variable (either stress or strain-rate) planes. The solid lines in Fig. 18 are analogous to lines of phase coexistence in, for example, the pressure-temperature plane in a simple fluid.

Consider Fig. 18(a). Here, $\hat\sigma_{xy}$ and μ are the proper field variables for phase separation at a common stress, and the solid lines denote the I-L and I-N phase boundaries. The dashed line denotes the range of stresses at coexistence for common strain-rate phase separation [Fig. 18(a)], for which stress is a generalized density variable and strain rate the field variable.

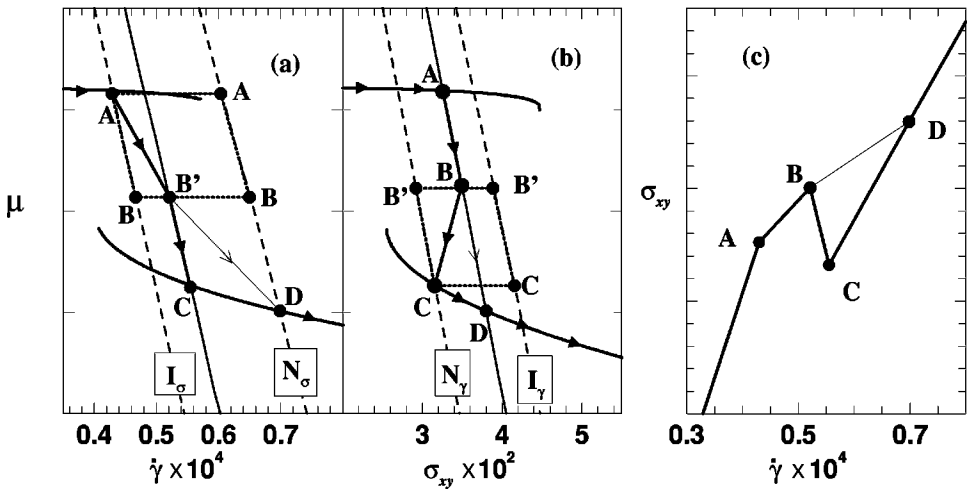

FIG. 19. Phase diagrams in the (a) μ-$\dot{\gamma}$ and (b) μ-σ_{xy} planes for I-N coexistence (the N state is stable for higher strain rate or stress, respectively). The thin vertical solid lines denote phase coexistence at common strain rate and stress in (a) and (b), respectively. The broken lines marked I_γ and N_γ denote the coexisting states at common strain rate in the μ-σ_{xy} plane (b), while the broken lines I_σ and N_σ denote the coexisting states at common stress, in the μ-$\dot{\gamma}$ plane. (c) is the mean stress vs strain-rate curve. Shown is a path A-B-C taken under the proposition that the system maintains a global minimum in chemical potential. Point A is at coexistence in the μ-σ_{xy} plane (b), and hence corresponds to two points, on lines I_σ and N_σ, in the μ-$\dot{\gamma}$ plane (a) for the two different strain rates of the coexisting phases. Similarly, point C corresponds to coexistence at common strain rate in (a), with the coexisting phases at different stresses lying on lines I_γ and N_γ in (b), at the two points C. Points B and B′ are coincident in (c), and correspond to a crossover from phase separation at common stress (B) to phase separation at common strain rate (B′). The path A-B-C in (c) may be traced in (b) by following the upper horizontal arrow until phase separation at common stress occurs at A, then along the segments A-B in (b) or A-B′ in (a) until phase separation at common strain rate occurs at B′. From this point until C the system phase separates along I_γ and N_γ, with a mean stress given by the thick diagonal solid arrow B-C in (b) and the thick segment B′-C in (a). The system emerges from the two-phase region at C on N_γ, and continues through D on the high strain rate branch.

Figure 18(a) indicates that, for a system undergoing I-N at a common strain rate, the chemical potential and stress for the I phase falls within the single phase N region of the common *stress* phase diagram. Hence, we expect this I phase to be unstable (or metastable) with respect to phase separation at common stress. Similarly, the control parameters (chemical potential and stress) for the N phase coexisting at a common strain rate lie within the single phase I region for common stress phase separation, which we also expect to be unstable (or metastable). Conversely, for a system coexisting at a common stress the I phase lies within the single phase I region of the common strain-rate phase diagram [Fig. 18(b)], and similarly for the N phase. This suggests that phase separation at a common strain rate is unstable (or metastable) with respect to phase separation at common stress, while phase separation at a common stress is stable.

Note that, ultimately, this selection of phase-coexistence geometries follows from the transition being a shear-thinning transition; for a shear-thickening transition the situation could be reversed. In this case phase coexistence at a common strain rate and a given μ would imply a shear-induced phase (analogous to the N phase) with a higher stress than the I phase. If the phase-coexistence line for common stress (strain rate) lay within a loop corresponding to the stresses (strain rates) for common strain-rate (stress) coexistence, then common strain-rate coexistence would be expected to be stable, by analogy with the isotropic-nematic shear thinning model. Obviously this argument is delicate. In a fluid where only one-phase coexistence (either common stress or common strain rate) is supported by the dynamical equations, this argument is moot.

An alternative possibility is presented in Fig. 19 if one argues that in steady state, among the possible phases which are compatible with the interface solvability condition, the chemical potential reaches its absolute minimum. Consider increasing the strain rate for a given mean concentration. The thick horizontal arrows in Figs. 19(a)–19(c) denote the $\mu(\sigma_{xy})$ and $\mu(\dot{\gamma})$ paths for the homogeneous high and low shear rate states, in the two phase diagrams. In Fig. 19(a) the path is A-B′-C-D, in Fig. 19(b) the path is A-B-C-D, and in Fig. 19(c) the path is A-B-C-D.

This path ensures that the system maintains the minimum chemical potential for an imposed strain rate. Upon increasing the strain rate from zero, the system remains in the one-phase region until A is reached, at which point phase separation at common stress occurs. Note that A spans two points of coexistence in the μ-$\dot{\gamma}$ plane [Fig. 19(a)] on the lines I_σ and N_σ. Upon further increasing the strain rate, the system continues to phase-separate at common stress, following the segment A-B in Fig. 19(b) and the two (coexisting) segments A-B in Fig. 19(a). The mean chemical potential and strain rate follow the diagonal segment A-B′ in Fig. 19(a). Upon increasing the *strain rate* above B, the system can continue to maintain its lowest chemical potential by phase separating with a common strain rate in the two phases, i.e., with shear bands in the vorticity direction. Hence, the system next follows the path B′-C in Fig. 19(a) (μ-$\dot{\gamma}$ plane) and the two coexisting paths B′-C in Fig. 19(b) (μ-σ_{xy} plane), with the mean chemical potential and stress following the diagonal segment B-C in Fig. 19(b). Finally, upon increasing the strain rate above C, the system continues along the high

strain-rate branch. The thin diagonal lines with arrows, B′-D in Fig. 19(a) and B-D in Fig. 19(b), show the path that would be taken if the system passed through the two-phase region entirely with a common stress in the two phases. This scenario follows from minimizing the chemical potential, and its correctness, of course, should be further examined by the full time evolution of the original dynamic equations.

It is probable that boundary conditions also play a role. Consider a Couette device. Typically the walls provide uniform boundary conditions in the azimuthal direction, while the slight inhomogeneity of Couette flow induces an asymmetry between the inner and outer cylinders. The slightly higher stress near the inner wall provides a preference for the high strain-rate nematic phase, and hence might enhance the stability of common stress phase separation. Similarly, the intrinsic inhomogeneity (although weaker) in cone-and-plate rheometry induces a preference for the common stress interfacial configuration [46].

We are also unable to say anything about the number or spacing of bands. Analogies with equilibrium systems suggest that phase separation would coarsen until the system formed two bands at different strain rates (for phase separation at a common stress). This is the behavior seen in visualizations of flow in Couette, cone-and-plate, and pipe geometries, where the intrinsic inhomogeneity provides a ''seed'' for macroscopic phase separation [2,44–47,52]. Recent visualization of banding in lamellar surfactant systems [38] indicates that phase separation at a common strain rate can exhibit bands (disklike bands in Couette flow) whose initial spacing depends on the applied strain rate and that coarsen in time. Unlike common stress bands, which are expected to (and do) form macroscopic bands in Couette flow, there is no boundary effect in Couette (aside from perhaps sedimentation) which would encourage common strain-rate bands to coalesce readily. Normal stresses may play a role in this process.

C. Stability at prescribed stress or prescribed strain rate

In calculating the phase diagrams, we have calculated the stability of the fluid under conditions of either fixed strain rate or fixed stress. These limits of stability, analogous to spinodals in equilibrium systems, are displayed in Figs. 8 and 14. Note that the stability limits and critical points differ, depending on the control variable (stress σ or strain rate $\dot{\gamma}$). To see why this is, note that schematically the dynamical equations of motion have the form

$$\partial_t \mathbf{x} = \mathbf{f}(\mathbf{x}, \dot{\gamma}), \tag{7.2}$$

$$\sigma = g(\mathbf{x}, \dot{\gamma}), \tag{7.3}$$

where $\mathbf{x}$ comprises the dynamical variables (order parameter $\boldsymbol{Q}$ and composition ϕ). The second equation relates the stress to strain rate and dynamical variables at steady state (or in the zero Reynolds number limit), which implies that the strain rate $\dot{\gamma}$, for a given stress, is a function $\dot{\gamma} = \dot{\gamma}(\sigma, \mathbf{x})$. Consider fluctuations about a steady state $\mathbf{x}_0$: $\mathbf{x} = \delta\mathbf{x} + \mathbf{x}_0$. The dynamics for the fluctuation obeys

$$\partial_t \, \delta\mathbf{x} = \left\{ \frac{\partial \mathbf{f}}{\partial \mathbf{x}} + \frac{\partial \mathbf{f}}{\partial \dot{\gamma}} \frac{\partial \dot{\gamma}}{\partial \mathbf{x}} \right\} \cdot \delta\mathbf{x} \tag{7.4}$$

$$\equiv \{ \mathsf{M}_\gamma + \delta \mathsf{M}_\sigma \} \cdot \delta\mathbf{x}. \tag{7.5}$$

The limit of stability for common strain rate is calculated using the fluctuation matrix M_γ, while the limit of stability for common stress was calculated using $\mathsf{M}_\gamma + \delta\mathsf{M}_\sigma$. These correspond to different stability criteria.

The question of which spinodal could be observed in an experiment relies on the accuracy of prescribed stress and prescribed strain-rate rheometers. For a rheometer operating at a prescribed strain rate, then if $\delta\mathbf{x}$ goes unstable through M_γ [in Eq. (7.2)], the stress increases due to Eq. (7.3) and no attempt is made to control it, leading to instability. However, consider a rheometer which maintains a prescribed stress. If the system goes unstable in Eq. (7.2), the bulk stress will change due to Eq. (7.3). A sensitive and fast enough rheometer will respond by adjusting the strain rate accordingly, to maintain the imposed stress. Hence, instability would be determined by the sum $\mathsf{M}_\gamma + \delta\mathsf{M}_\sigma$.

Similarly, in equilibrium systems a locus of stability may be defined by, for example, the diverging of isothermal or adiabatic or isobaric or isochoric response functions (or the vanishing of the appropriate modulus). For example, the isothermal and adiabatic compressibilities K_T and K_S differ by a term proportional to the quotient of the square of the thermal expansion coefficient α_p and the isobaric heat capacity c_p:

$$K_T - K_S = \frac{v T \alpha_p^2}{c_p}, \tag{7.6}$$

where v is the specific volume. K_T^{-1} vanishes along the spinodal line $v_s(T)$, while it is evident that K_S^{-1} (proportional to the sound speed) does not. However, in equilibrium, the critical point is uniquely defined in phase space, which is related to the fact that, for example, pressure is a unique *function* of the volume, and is in fact a state variable. Conversely, we can see from the shape of the stress–strain-rate curves for the Doi model [e.g., Figs. 3(c)–3(e)], that the stress can be a multivalued function of strain rate; i.e., it is not a state function. Hence there is no compelling reason to expect critical points at imposed strain rate to be the same as critical points at imposed stress. Similarly, the *true* spinodal or locus of stability is uniquely defined in an equilibrium system because of the convexity requirement on the entropy [72], and there is no such universal convexity requirement (barring entropy production, which is minimized only under restricted conditions, and only locally rather than globally) for nonequilibrium systems.

D. An analogy with equilibrium systems?

The liquid crystalline suspension under flow, indeed any system which undergoes a macroscopic bulk flow-induced phase transition, is analogous to an equilibrium ternary system comprising species *A*, *B*, and solvent. In our case, the roles of *A* and *B* are played by the rigid-rod composition ϕ and either the stress σ or strain rate $\dot{\gamma}$, depending on the nature of the phase separation. For phase separation at common stress, the phase diagram in the stress-composition

plane σ-ϕ is analogous to the μ_A-ϕ_B plane for the equilibrium system, while the $\dot{\gamma}$-ϕ plane is analogous to the ϕ_A-ϕ_B plane. In either case, the density variables, $\{\dot{\gamma},\phi\}$ in flow and $\{\phi_A,\phi_B\}$ in the analogous equilibrium system, are different in the two coexisting phases. The slope of the ''plateau'' in the σ-$\dot{\gamma}$ plane, as the system traverses the two-phase region of the phase diagram, is analogous to a slope in the μ_A-ϕ_B plane, the latter indicating that the chemical potential (or osmotic pressure) of the two phases varies across the coexistence region.

Can this analogy be extended to the possibility of phase separation at common stress *or* common strain rate? Certainly, one can consider a ternary system under conditions of either imposed ϕ_A or imposed μ_A, for which one generally expects difference spinodal lines. That is, the spinodal is determined by the instability of a matrix in the two-dimensional space spanned by ϕ_A and ϕ_B, and fixing ϕ_A or μ_A projects this instability onto different subspaces. Experimental conditions may dictate that the spinodal line under fixed ϕ_A is more likely to be seen, since ϕ_A is conserved and cannot equilibrate quickly to satisfy an imposed μ_A. However, we are not aware of any ternary equilibrium system for which the equilibrium coexistence conditions can differ; that is, equilibrium is *always* specified by equality of μ_A and μ_B in the two phases, and never by equality of ϕ_A.

VIII. SUMMARY

In this work we have proposed a straightforward phenomenological extension to the Doi model for a solution of rigid-rod particles. We have added entropic terms and included inhomogeneous terms in order to calculate phase separation in shear flow. The main results of this study are as follows.

(i) Phase separation may occur under conditions of common stress *or* common strain rate, with different interface orientations with respect to flow geometry for the two cases.

(ii) Although both phase separations are possible, the phase diagrams in the μ-σ_{xy} and μ-$\dot{\gamma}$ planes (Fig. 18) suggest that phase separation at a common strain rate is metastable. This can be traced, for this model, to the shear-thinning character of the transition. For a shear-thickening transition an equivalent argument suggests that (if both are kinematic possibilities) common stress phase separation is metastable with respect to strain-rate phase separation.

(iii) The limits of stability (''spinodals'') and critical points for systems at prescribed stress and prescribed strain rate differ; the difference of spinodals is similar to equilibrium behavior, while the difference of critical points is related to the fact that neither stress or strain rate are always unique state functions.

(iv) An argument based on minimizing the chemical potential predicts a complex crossover from common stress to common strain-rate phase separation for controlled strain-rate experiments. The veracity of this assumption is unknown.

(v) We have calculated phase coexistence among three phases (paranematic I, flow-aligning nematic N, and log-rolling nematic L), where only two phases existed in equilibrium. We expect I-N phase coexistence to be the stable configuration (Fig. 13), although I-L phase coexistence could exist as a metastable state with approprate preparation. We do not expect three-phase coexistence for this model.

(vi) We have demonstrated how to calculate the mean stress–strain-rate relationship $\overline{\sigma}(\overline{\dot{\gamma}})$ in the coexistence region. The shape of $\overline{\sigma}(\overline{\dot{\gamma}})$ is determined by the composition and strain rates of the coexisting phases [28].

(vii) A phase-separated system can exhibit an apparently unstable constitutive relation, with negative slope $\partial\sigma_{xy}/\partial\dot{\gamma}$. Experiments have accessed such negative slope composite curves under controlled stress (rather than controlled strain-rate) conditions [69].

(viii) Our method of solution is general and relies on the existence of a set of dynamical equations of motion for the structural order parameter of the particular transition, including the dynamic response to inhomogeneities.

(ix) For $\lambda = g/K$ finite, the phase boundaries we have found are, within our accuracy, independent of the relative magnitude of the gradient terms in our free energy. Although this suggests that, for the restricted set of inhomogeneities we have incorporated, a selection criterion exists involving only the homogeneous equations of motion, this is not true in general for complex fluids in flow [35]. For $\lambda=\infty$, the phase boundaries are slightly shifted.

(x) Studies at different aspect ratios suggest that shear flow enhances polydispersity effects relative to their effect on equilibrium phase boundaries.

We close by enumerating several open questions. First, systems such as wormlike micelles probably possess some combination of a perturbed isotropic-nematic transition and a dynamic instability of the molecular constitutive relation. It is conceivable that suitable compositions of these systems could yield a stress–strain-rate composition surface (Fig. 4) with multiple folds. Second, it would be desirable to have a model shear-thickening system in which to calculate properties of banded flows, to compare and contrast with the shear-thinning system studied here and to understand experiments on a wide range of systems, including clays and surfactant systems. Third, we have not addressed the number and possible coarsening of bands and band configurations, and the kinetics of phase separation has hardly been treated theoretically [2], with experiments also at an early stage [2,29,51]. Finally, we do not yet know the conditions which may, if at all, distinguish between common stress or common strain-rate phase coexistence.

ACKNOWLEDGMENTS

It is a pleasure to acknowledge helpful conversations and correspondence with R. Ball, J.-F. Berret, G. Bishko, D. Bonn, M. Cates, F. Greco, J. Harden, S. Keller, G. Leal, T. McLeish, D. Pine, G. Porte, O. Radulescu, N. Spenley, L. Walker, and X.-F. Yuan. C.-Y.D.L. acknowledges funding from St. Catharine's College, Cambridge and the (Taiwan) National Science Council (NSC 88-2112-M-008-005).

[1] J.F. Berret, D.C. Roux, G. Porte, and P. Lindner, Europhys. Lett. **25**, 521 (1994).
[2] J.F. Berret, D.C. Roux, and G. Porte, J. Phys. II **4**, 1261 (1994).
[3] J.F. Berret, G. Porte, and J.P. Decruppe, Phys. Rev. E **55**, 1668 (1997).
[4] S. Hess, Z. Naturforsch. A **31a**, 1507 (1976).
[5] P.D. Olmsted and P.M. Goldbart, Phys. Rev. A **41**, 4578 (1990).
[6] P.D. Olmsted and P.M. Goldbart, Phys. Rev. A **46**, 4966 (1992).
[7] P.T. Mather, A. Romo-Uribe, C.D. Han, and S.S. Kim, Macromolecules **30**, 7977 (1997).
[8] H. See, M. Doi, and R. Larson, J. Chem. Phys. **92**, 792 (1990).
[9] P.D. Olmsted and C.-Y.D. Lu, Phys. Rev. E **56**, 55 (1997).
[10] C.R. Safinya, E.B. Sirota, and R.J. Plano, Phys. Rev. Lett. **66**, 1986 (1991).
[11] M.E. Cates and S.T. Milner, Phys. Rev. Lett. **62**, 1856 (1989).
[12] D. Roux, F. Nallet, and O. Diat, Europhys. Lett. **24**, 53 (1993).
[13] O. Diat, D. Roux, and F. Nallet, J. Phys. II **3**, 1427 (1993).
[14] O. Diat, D. Roux, and F. Nallet, Phys. Rev. E **51**, 3296 (1995).
[15] G.H. Fredrickson, J. Rheol. **38**, 1045 (1994).
[16] M. Goulian and S.T. Milner, Phys. Rev. Lett. **74**, 1775 (1995).
[17] K.A. Koppi *et al.*, J. Phys. II **2**, 1941 (1992).
[18] K.I. Winey, S.S. Patel, R.G. Larson, and H. Watanabe, Macromolecules **26**, 2542 (1993).
[19] R.M. Kannan and J.A. Kornfield, Macromolecules **27**, 1177 (1994).
[20] M. Doi and S. F. Edwards, *The Theory of Polymer Dynamics* (Clarendon, Oxford, 1989).
[21] M.E. Cates, T.C.B. McLeish, and G. Marrucci, Europhys. Lett. **21**, 451 (1993).
[22] N.A. Spenley, M.E. Cates, and T.C.B. McLeish, Phys. Rev. Lett. **71**, 939 (1993).
[23] M.E. Cates, J. Phys. Chem. **94**, 371 (1990).
[24] H. Rehage and H. Hoffmann, Mol. Phys. **74**, 933 (1991).
[25] T.C.B. McLeish and R.C. Ball, J. Polym. Sci., Part B: Polym. Phys. **24**, 1735 (1986).
[26] A.Y. Zubarev, Colloid J. USSR **58**, 189 (1996).
[27] G. Porte, J.F. Berret, and J.L. Harden, J. Phys. II **7**, 459 (1997).
[28] V. Schmitt, C.M. Marques, and F. Lequeux, Phys. Rev. E **52**, 4009 (1995).
[29] C. Grand, J. Arrault, and M.E. Cates, J. Phys. II **7**, 1071 (1997).
[30] F. Greco and R.C. Ball, J. Non-Newtonian Fluid Mech. **69**, 195 (1997).
[31] P. Español, X.F. Yuan, and R.C. Ball, J. Non-Newtonian Fluid Mech. **65**, 93 (1996).
[32] P. D. Olmsted, O. Radulescu, and C.-Y. D. Lu, J. Rheol. (to be published).
[33] J.R.A. Pearson, J. Rheol. **38**, 309 (1994).
[34] N.A. Spenley, X.F. Yuan, and M.E. Cates, J. Phys. II **6**, 551 (1996).
[35] C.-Y. D. Lu, P. D. Olmsted, and R. C. Ball (unpublished).
[36] J. L. Goveas and G. H. Fredrickson, J. Rheol. (to be published).
[37] J. K. G. Dhont, Phys. Rev. E **60**, 4544 (1999).
[38] D. Bonn *et al.*, Phys. Rev. E **58**, 2115 (1998).
[39] A.V. Bhave, R.K. Menon, R.C. Armstrong, and R.A. Brown, J. Rheol. **37**, 413 (1993).
[40] M. Doi, J. Polym. Sci., Part B: Polym. Phys. **19**, 229 (1981).
[41] N. Kuzuu and M. Doi, J. Phys. Soc. Jpn. **52**, 3486 (1983).
[42] P. D. Olmsted and C.-Y. D. Lu, Faraday Discuss. **112**, 183 (1999).
[43] V. Schmitt, F. Lequeux, A. Pousse, and D. Roux, Langmuir **10**, 955 (1994).
[44] P.T. Callaghan, M.E. Cates, C.J. Rofe, and J.B.A.F. Smeulders, J. Phys. II **6**, 375 (1996).
[45] R.W. Mair and P.T. Callaghan, Europhys. Lett. **36**, 719 (1996).
[46] M.M. Britton and P.T. Callaghan, Phys. Rev. Lett. **78**, 4930 (1997).
[47] R.W. Mair and P.T. Callaghan, J. Rheol. **41**, 901 (1997).
[48] P. van der Schoot, Macromolecules **27**, 6473 (1994).
[49] D.C. Roux *et al.*, Macromolecules **28**, 1681 (1995).
[50] E. Cappelaere *et al.*, Phys. Rev. E **56**, 1869 (1997).
[51] J.F. Berret, Langmuir **13**, 2227 (1997).
[52] P. Boltenhagen, Y.T. Hu, E.F. Matthys, and D.J. Pine, Europhys. Lett. **38**, 389 (1997).
[53] P. Boltenhagen, Y.T. Hu, E.F. Matthys, and D.J. Pine, Phys. Rev. Lett. **79**, 2359 (1997).
[54] S.L. Keller, P. Boltenhagen, D.J. Pine, and J.A. Zasadzinski, Biophys. J. **72**, TU428 (1997).
[55] R. B. Israel, *Convexity in the Theory of Lattice Gases* (Princeton University Press, Princeton, 1978).
[56] L. D. Landau and E. M. Lifschitz, *Statistical Physics, 3rd Edition, Part 1* (Pergamon, Oxford, 1980).
[57] P.A. Buinen and H.N.W. Lekkerkerker, J. Phys. Chem. **97**, 11 510 (1993).
[58] A.W. El-Kareh and L.G. Leal, J. Non-Newtonian Fluid Mech. **33**, 257 (1989).
[59] L. Kramer, Z. Phys. B **41**, 357 (1981).
[60] Y. Pomeau, Physica D **32**, 3 (1986).
[61] C.V. Chaubal, L.G. Leal, and G.H. Fredrickson, J. Rheol. **39**, 73 (1995).
[62] T.C. Lubensky, Phys. Rev. A **2**, 2497 (1970).
[63] P. G. de Gennes and J. Prost, *The Physics of Liquid Crystals*, 2nd ed. (Clarendon, Oxford, 1993).
[64] T. Odijk, Liq. Cryst. **1**, 553 (1986).
[65] J. D. Gunton, M. S. Miguel, and P. S. Pahni, *Phase Transitions and Critical Phenomena* (Academic Press, New York, 1983), Vol. 8, p. 267.
[66] P. M. Chaikin and T. C. Lubensky, *Principles of Condensed Matter Physics* (Cambridge Unviersity Press, Cambridge, 1995).
[67] O. G. Radulescu and P. D. Olmsted, J. Non-Newtonian Fluid Mech. (to be published).
[68] Y.Y. Renardy, Theor. Comput. Fluid Dyn. **7**, 463 (1995).
[69] Y.T. Hu, P. Boltenhagen, and D.J. Pine, J. Rheol. **42**, 1185 (1998).
[70] D. Zwillinger, *Handbook of Differential Equations* (Academic Press, London, 1997).
[71] A.J. Liu and G.H. Fredrickson, Macromolecules **26**, 2817 (1993).
[72] P. G. Debenedetti, *Metastable Liquids: Concepts and Principles* (Princeton University Press, Princeton, 1996).